Chen *et al. Energy Mater* 2023;3:300045
DOI: 10.20517/energymater.2023.35

Energy Materials

Review

Open Access

Check for updates

Research on carbon-based and metal-based negative electrode materials via DFT calculation for high potassium storage performance: a review

Yuefang Chen[1,3], Heyi Sun[1], Junpeng Guo[1], Yuwen Zhao[1], Huan Yang[1], Hongwei Li[1,3], Wei-Jie Li[2,*], Shulei Chou[3], Yong Jiang[1], Zhijia Zhang[1,*]

[1]State Key Laboratory of Separation Membrane and Membrane Processes, School of Materials Science and Engineering, Tiangong University, Tianjin 300387, China.
[2]Powder Metallurgy Research Institute, Central South University, Changsha 410083, Hunan, China.
[3]Institute for Carbon Neutralization, College of Chemistry and Materials Engineering, Wenzhou University, Wenzhou 325035, Zhejiang, China.

[*]**Correspondence to:** Prof. Zhijia Zhang, State Key Laboratory of Separation Membrane and Membrane Processes, School of Materials Science and Engineering, Tiangong University, 399 Binshui West Road, Tianjin 300387, China. E-mail: zhangzhijia@tiangong.edu.cn; Prof. Wei-Jie Li, Powder Metallurgy Research Institute, Central South University, Hongyuan Road, Changsha 410083, Hunan, China. E-mail: li-306@csu.edu.cn

How to cite this article: Chen Y, Sun H, Guo J, Zhao Y, Yang H, Li H, Li WJ, Chou S, Jiang Y, Zhang Z. Research on carbon-based and metal-based negative electrode materials via DFT calculation for high potassium storage performance: a review. *Energy Mater* 2023;3:300045. https://dx.doi.org/10.20517/energymater.2023.35

Received: 30 Apr 2023 **First Decision:** 29 May 2023 **Revised:**15 Jun 2023 **Accepted:** 27 Jun 2023 **Published:** 12 Oct 2023

Academic Editors: Federico Bella, Wei Tang **Copy Editor:** Fangyuan Liu **Production Editor:** Fangyuan Liu

Abstract

The key R&D concern in the domain of new energy in recent years has been the large-scale development of electrochemical energy storage. However, the steep increase in pricing has constrained the further expansion of lithium-ion batteries, primarily due to the ongoing depletion of their scarce lithium supplies. A potential candidate material at the moment is the potassium-ion battery (KIB), which has an anode made of carbon and/or an alloy and rich reserves, offering an excellent theoretical capacity and ideal working voltage. More significant advancements are still required to achieve long life and high energy density, despite the fact that some significant breakthroughs have been reported. The most recent findings from research on carbon-based [graphite, hard carbon (HC), and nanoporous carbon] and alloy-based (mainly including Sb, Sn, P, and its compounds) anodes for KIBs are compiled in this document. Numerous simulations at the atomic level based on particular chemical interactions, phase transitions, ion/electron transport dynamics, and conduction band spin utilizing density functional theory (DFT) calculations have been conducted to thoroughly investigate the storage mechanism of K^+ on various electrode materials. Moreover, this paper examined contemporary structural modification techniques

used in carbon- and alloy-based anode electrode materials and applied DFT calculations to confirm the advancement of its thorough tests. To promote the manufacturing of rechargeable KIBs, the challenges and potential of KIBs were also explored in future research.

Keywords: Carbon-based anode, alloy-based anode, electronic structure, DFT theory, potassium-ion battery

INTRODUCTION

The massive consumption of fossil fuels and the growing environmental problems have prompted the rapid growth of the demand for clean energy in human society[1,2]. Therefore, it is imperative to develop secondary batteries to promote the progress of large-scale energy storage technology and realize the efficient use of energy[3]. Lithium-ion batteries (LIBs), as secondary batteries, have been commercialized in electric vehicles, energy storage, and other fields due to their high reversible specific capacity, cycle stability, and other advantages[4]. However, lithium resources in the earth are low in reserves and expensive, which is not suitable for large-scale energy storage devices. In various alternative battery systems, the abundant reserves of sodium (Na) and potassium (K) have become research hotspots due to their chemical properties and working principles similar to LIBs. However, as an alkali metal, K-ion batteries (KIBs) have faced more competition than LIBs and sodium-ion batteries (NIBs) due to the low-cost and suitable standard potential of K/K^+, which has been extensively investigated and considered as the promising energy storage technology.

For KIBs, the most outstanding benefit is the low redox potential of K/K^+, which gives rise to a high energy density and makes it possible to design high output voltage[5]. In addition, due to a much larger ionic radius of K^+ (0.138 nm) compared to Li^+ (0.076 nm) and Na^+ (0.102 nm), KIBs exhibit low charge density and Lewis acidity, resulting in weak interactions and low desolvent activation energy. But in addition to allowing for high ionic transport, weak interactions between K^+ ions and solvent molecules with smaller Stokes radii can also result in fast rates due to lower desolvent activation energies. Thanks to the aforementioned advantages, anode materials for KIBs, such as carbon-based anodes, alloys, oxides, sulfides, selenides, and more, exhibit excellent potassium storage capacity and cycling stability.

In the past few decades, systematic research on KIBs has become the main focus of researchers both domestically and internationally. As the next alkali metal after sodium, potassium has a lower oxidation-reduction potential. Since KIBs work at a higher potential, it is conducive to improving energy density. In addition, there is a weak interaction between K^+ and solvent molecules with a smaller Stokes radius, and a lower desolvent activation energy can improve the ion transport rate. On the other hand, the intercalation/detachment mechanism of K^+ with graphite is believed to be similar to lithium, mainly through the formation of graphite intercalation compounds in stages. With the increase of K concentration, KC_8 is ultimately formed[6]. Among them, anode materials, as an important component of KIBs, including carbon materials [graphene, carbon microspheres, carbon nanofibers (CNFs)], metal alloys, oxides, sulfides, and other materials[7], have been proven to contribute to the development of high-performance KIBs [Figure 1A]. In terms of cost [Figure 1B], carbon-based materials stand out among a group of candidate materials due to their advantage of very low cost, becoming one of the preferred anode materials for commercial KIBs. Unfortunately, the larger ionic radius makes it more difficult for K^+ to be embedded in the electroactive material, resulting in a slow kinetic behavior of the K^+ reaction in the solid electrode. Controlling the size of the material and preparing nanostructured materials can effectively improve the K^+ reaction kinetics and further enhance the rate capability[8]. On the other hand, the insertion/removal of large-sized K^+ can easily cause significant volume expansion of the electrode material during the potassium

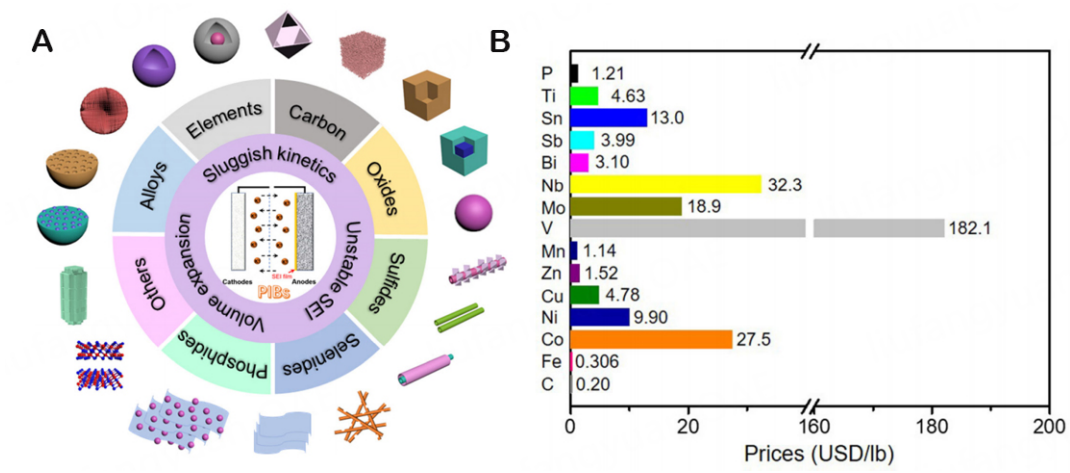

Figure 1. (A) Overview of the proposed architectures for serving as the anodes of PIBs. (B) Price comparison of various metals for potential applications in PIBs. Copyright 2021, Nano Research[7].

process[9]. Thus, researchers continuously attempt to design and optimize electrode materials, electrolytes, and electrode components and structures in a reasonable manner[10,11].

Moreover, the comprehension and identification of potassium storage materials can be assisted by simulations[12,13]. In this review, the following quantities of interest can be calculated via systematic density functional theory (DFT) computations[14,15]: the structure-property correlation, interfacial stability, phase transition, K^+ adsorption and diffusion mechanisms of electrode materials, along with spin correlation effects triggered by some metal atom doping[16,17]. Since the creation of KIBs, there has been a lot of emphasis on the development of ultra-high-performance anodes, such as intercalation type carbonaceous-based anodes manufactured of graphite, HC, and soft carbon, as well as alloy-based materials made of transition metal nitrides, oxides, and sulfides. From this perspective, we examine the modeling literature for two significant groups of potassium storage materials, carbon-based systems and alloy-based systems. Finally, we present a future outlook in anode material development for KIBs.

CARBON-BASED ANODES FOR KIBS

Anode materials, as critical components of KIBs, directly affect the battery performance, including operating potential and cyclability. Owing to a significantly higher ionic radius of K^+, seeking appropriate potential electrode materials has become crucial for the development of KIBs. Among them, carbon-based materials have been successfully used as anode materials in KIBs due to their plentiful sources, environmentally friendly nature, low cost, and good chemical inertia, which is due to the similar physical and chemical properties of lithium and potassium. In this section, we divided anode materials into three categories according to the storage mechanisms of K^+, which consist of graphite-based anodes, HC-based anodes, and nanoporous carbon composite anodes.Graphite-based anode for KIBs.

Nowadays, graphite has been the dominant supplier for LIB anodes attributed to its low cost, low (de-)lithiation potentials, high intrinsic capacity, and limited volume change during the (de-)lithiation process. Lithium can be inserted into graphite, leading to the formation of LiC_6, which represents the stage-one Li-graphite intercalation compound (GIC) and has a 370 mAh/g reversible capacity[18]. Therefore, considering the success of graphite in the LIB industry, it is crucial to evaluate the electrochemical performance of graphite electrode material in KIBs. Research has shown that anode materials with superior

potassium storage performance include metals, oxides, sulfides, phosphides, *etc*[19]. However, the enhancement of energy density in KIBs is constrained by decreased cycle stability and a large voltage plateau. In KIBs, with the formation of KC_8, K/graphite batteries can generate a physical specific capacity of approximately 279 mAh/g[20]. However, the small interlayer spacing of graphite is not conducive to the intercalation behavior of large ions, such as Na^+ and K^+, resulting in slow charging and discharging dynamics and poor storage capacity[21]. In order to improve the energy storage capabilities of KIBs, structural engineering techniques have been used to create advanced graphite-based materials, such as expanded graphite (EG)[22], GICs[23], and porous graphite (PG)[24]. By inserting functional groups containing oxygen (O), EG, a graphite-based material, primarily increases the layer gap of layered graphite nanosheets. More active sites can be provided by the wider layer spacing and O-containing groups, which can enhance the storage capacity of metal ions. While preserving weak van der Waals bonds between the graphite layers, the space created by the insertion of guest molecules between the graphite layers makes up the majority of GICs. The strong interaction of guest molecules with graphite layers can make metal ions more electronically conductive. As a modified form of graphite, PG gains from the additional ion diffusion channels that are provided by its distinctive porous structure, which also acts as a buffer against structural deformation during charging and discharging operations. Additionally, as a crucial part of KIBs, electrolytes have drawn a lot of interest from researchers[25]. The performance of KIBs is significantly influenced by the kind and quantity of salt, solvents, and electrolyte additions[26]. However, the effects of additives on the functionality of KIBs have received comparatively little attention. Hence, the structural engineering of electrolytes will be the research area of future development. To introduce the co-intercalation mechanism and accomplish the high potassium storage performance of KIBs, a suitable electrolyte will need to be identified.

At the same time, plenty of literature indicated that graphite can intercalate potassium, which prompted more studies into the creation of KIBs. Furthermore, Komaba *et al.* have demonstrated the production of KC_8 GICs in stage I based on the potassium reaction of graphite in carbonate-based electrolytes, which can provide a high specific capacity of 244 mAh/g[27]. In 2015, Jian *et al.* conducted the first research focusing on the electrolytic K^+ insertion behavior in graphite for non-aqueous electrolytes[9]. The (de-)potassiation mechanism in graphite was revealed and shown in Figure 2A, and the quasi-equilibrium potentials of (de-)potassiation are much higher than those of the (de-)lithiation process, which is essential since it decreases the formation of potassium dendrites during the potassiation process[28]. In Figure 2B, it can be observed that when KC_8 is generated, the depotassiation capacity is extremely close to its theoretical value of 279 mA h/g. The initial Coulombic efficiency (ICE) of 57.4% is a result of the initial potassiation capacity exceeding the predicted capacity significantly.

Ex situ X-ray diffraction (XRD) has been employed to support the potassium storage mechanism in graphite, which contains the formation of several stages of K-GICs, including stage-3 KC_{36}, stage-2 KC_{24}, and stage-1 KC_8 [Figure 2C]. The number of graphene layers that separate the neighboring layer of the K-intercalated layer determines the sequence of stage K-GICs along the axis. After potassium oxidation, the graphite diffraction peak still exists in the range of 0.3 V to 0.2 V, and the appearance of additional peaks can be attributed to the presence of KC_{36}, which is shown in Figure 2D. Each third pair of the host graphenes in KC_{36} has a layer of potassium [Figure 2E]. New peaks around 20.2° and 30.6° are seen when KC_{36} converts into KC_{24}, the stage-2 K GIC, after more potassiation (point 5). Phase-pure KC_8, the stage-1 K-GIC, emerges at 0.01 V following a two-phase period (points 6 and 7), so it exhibits distinctive XRD peaks at 16.4° and 33.4°. The decreased intensity of EG XRD peaks upon depotassiation implies that the potassium insertion triggered some volume expansion (by around 61%).

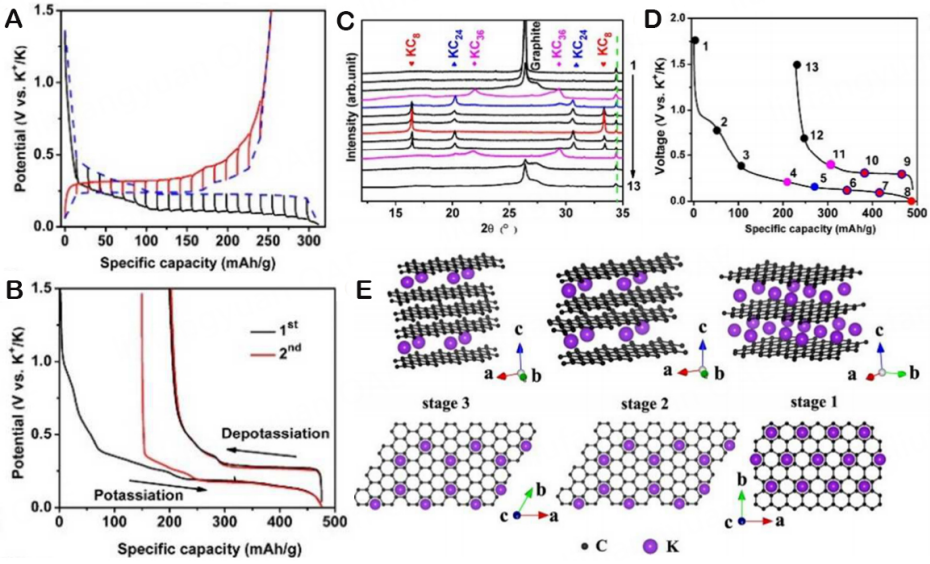

Figure 2. (A) Galvanostatic intermittent titration technique (GITT) curves of graphite at C/10. (B) Galvanostatic potassiation/depotassiation (GPD) profiles of graphite for the initial two cycles at C/40. (C) *Ex-situ* XRD patterns of (de-)potassiation of graphite corresponding to the voltage points in (D). (D) The first charge-discharge curve of graphite at C/10. (E) Schematic diagram of different K-GICs. Copyright 2015, American Chemical Society[9].

Through DFT calculations, a related investigation on K^+ insertion into graphite reveals a distinct manner for potassium insertion. Despite the fact that intercalation happens within three phases, Luo *et al.* posits that the development of stage-III (KC_{24}) accompanied by stage-II (KC_{16}) and stage-I (KC_8) is firmer than that of stage-III (KC_{36}) to stage-II (KC_{24}) and stage-I (KC_8), which is similar to lithium [Figure 3A][29]. It is vital to recognize that this is the first time to produce KC_8 at room temperature utilizing an electrochemical approach. Figure 3B shows a rather smooth potential slope ranging from 0.35 V to 0.18 V, corresponding to a capacity of only 93 mA h/g, which is connected to the stage-III (KC_{24}). A closer look reveals that the conversion of stage-II (KC_{16}) occurs at another shift around 0.14 V. Roughly 270 mA h/g is the whole first intercalation capacity, which points to the synthesis of stage-I (KC_8). These results seem to declare that the stage of K intercalation into graphite behaves similarly to that of Li intercalation. According to DFT analysis, the most stable stoichiometry is KC_8. As shown in Figure 3C, the potential must be negative to produce potassium metal; hence KC_6 cannot form in the potential window (2-0.01 V *vs.* K^+/K). When examining the staging process Stage-II (KC_{24}), Stage-I (KC_8) with results to DFT calculation (green line), we find that not just Stage-II (KC_{24}) (theory b) about 0.1 eV less solid than Stage-III (KC_{24}) (theory a), but the potential profile also exhibits a higher voltage from Stage-II (KC_{24}) to Stage-I KC_8, which is not observed in the experiment. Conversely, the energy grading mechanism from stage-III (KC_{24}) to stage-II (KC_{16}) and then to stage-I (KC_8) can maximize the separation of coulomb repulsion between ions (blue line). This fits the prospective profile we discovered through our experiments extremely well (black solid line and averaged red dotted line). Nevertheless, plenty of efforts have been devoted to solving challenges for KIBs, such as serious volume expansion and high irreversible capacity in the initial cycles due to large ionic radius. In 2022, Li *et al.* created a Graphdiyne/Graphene/Graphdiyne (GDY/Gr/GDY) composite structure for KIBs, which effectively improved the specific capacity thanks to its high specific surface area and active load[30]. In addition, a series of electrochemical characterizations were used to further investigate the storage mechanism of K ions, and the structural changes of GDY/Gr/GDY electrodes during repeated potassium/potassium removal processes were simulated in Figure 3D. Volume changes can be efficiently reduced, and structural integrity can be maintained by a greater interlayer gap and particular porous structure. As seen in Figure 3E, Yuan *et al.* created modified graphite (MG) to enable quick storage of K ions[31]. The optimized

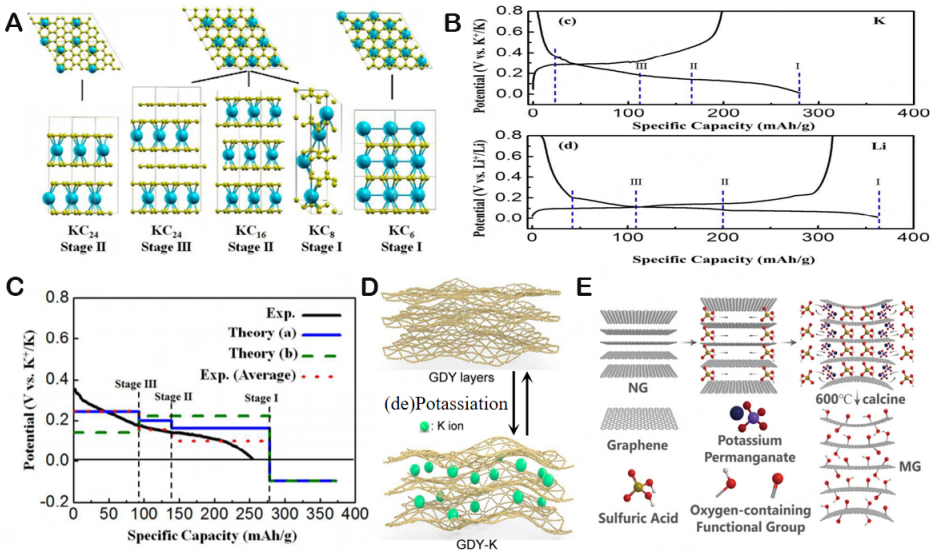

Figure 3. (A) Diagram illustrating the several stages of K-intercalated graphite, with K represented in blue and C shown in yellow. (B) The charge-discharge curves of K^+ and Li^+ embedded in graphite at ambient temperature and pressure, respectively. (C) Potential distribution of K^+ embedded in graphite at different stages based on DFT calculation. The interlayer stage is represented by the blue line [Theory (a)]: Stage-III (KC_{24}) → Stage-II (KC_{16}) → Stage-I (KC_8). The dotted green line [Theory (b)] represents the computed value of the phase that was previously reported: Stage-II (KC_{24}) → Stage- I (KC_8). The red dotted line is used to correct the capacitance contribution formed by SEI. Copyright 2015, Nano Letters[29]. (D) Schematic diagram of the potassium/dipotassium process in the GDY layer. Copyright 2022, ACS Nano[30]. (E) Schematic illustration of the preparation process for MG. Copyright 2021, Carbon[31].

MG anode material can maintain a capacity retention rate of 75% when assembled with Prussian Blue cathodes in the entire battery. In view of the controversial potassium storage mechanism of a graphite/potassium system, further research is needed to establish an optimal system for simulating the K^+ insertion and K^+ stripping process at various current rates.

Graphite has been successfully discovered and marketed as an anode for LIBs. However, the insertion and removal of K^+ during the electrochemical process limit the practical application of KIBs to poor cycling stability and severe volume expansion. Therefore, it is urgent to develop new modification strategies to improve the stability of graphite anodes. Hence, Capone *et al.* reported red phosphorus (RP)-graphite composite manufactured by a two-step ball-milling process in order to regulate particle size and maximize the carbon coating[32]. Raman measurements suggest that the volume expansion of RP particles causes the carbon covering to reversibly expand and shrink. Then, Ma *et al.* used triphenylphosphine and graphite oxide to prepare active phosphorus (P) and O double-doped graphene (PODG) for KIB anodes by a thermal annealing process[33]. Due to larger interlayer spacing, which accelerates the insertion and extraction of K^+, PODG exhibits high specific capacity and ultra-long cycling stability. In addition, the electrochemical performance of KIB graphite carbon anodes regulated by defect engineering has been further confirmed by DFT calculations. The preferred technique is nitrogen (N) doping since cutting-edge N dopants may efficiently increase the adsorption energy towards K^+ ions. A number of modification strategies for N-doped carbon-based materials have been applied over the last five years to create KIBs with superior K^+ storage performance. In order to establish a special symbiosis between great reversible K ion storage capacity and excellent recycling capacity, Lee *et al.* discovered activated crushed stone graphene (A-CG) with morphological and functional flaws through the aerosol spraying process and continuous reduction and activation technology[34]. The unique defect engineering enables A-CG materials to exhibit a high reversible capacity of 340 mAh/g. The greater K^+ adsorption energy at the defect site is one of the primary factors contributing to the improved performance of electrode materials, according to DFT simulation data. Single

vacancy (SV), double vacancy (DV), and Stone-Wales (SW) are typical flaws[35]. Furthermore, Zeng *et al.* synthesized flexible N and O dual-doped carbon-coated graphene foam films (denoted as NOC@GF) that achieve exceptional electrochemical performance for KIBs, delivering outstanding rate capability and reversible capacity[11]. Additionally, DFT analysis demonstrates that N-O dual-doping offers additional active sites, which is significant in enhancing the K^+ migration rate. As shown in Figure 4A, various values of the corresponding adsorption energies (E_{ads}) show that N, O co-doped structures are substantially more suitable for adsorbing K atoms than graphene alone. Aside from that, the differential charge density map reveals the charge transfer between K atoms and adjacent carbon atoms, while the accumulation of more charges near the N and O doping sites in the NOC layer provides a theoretical basis for improving the potassium storage performance of the electrode material [Figure 4B]. Figure 4C is the diffusion barrier study of K ions on graphene and doped graphene systems. These findings indicate that the lower E_d value on Graphene makes the electrolyte ions have a faster migration rate, and the excellent electrochemical performance of NOC@GF materials positions them as one of the candidate materials for KIBs.

To further interpret the relationship between electrochemical properties and the K^+ storage mechanism, Sun *et al.* theoretically calculated adsorption energy of K^+ on N-doped, O-doped, and N/O co-doped structures based on the DFT theory[28]. Among them, N/O co-doped graded porous carbon (NOPC) is carbonized with cyanobacteria as the carbon source, which shows excellent rate performance and potassium storage capacity in KIBs. During DFT simulation, K^+ is positioned at different positions for adsorption energy calculation. The results indicate that N-doped and N/O co-doped materials have smaller adsorption energy values. In addition, a series of theoretical calculations, including electron density and differential charge, further proved that the N/O co-doped structure is more conducive to K^+ adsorption, which theoretically supports the superior potassium storage effect of NOPC. There is still much to be undertaken before the atomic-doped defect graphite is widely developed and used, even though it displays adequate cycling performance and stability.

Hard carbon-based anode for KIBs

Given its affordable price, eco-friendliness, and high cycle stability, non-graphite carbon, which includes HC, soft carbon, and amorphous carbon, has become one of the potential candidate anodes in KIBs. Even if it is carbonized at an annealing temperature higher than 3,000 °C, HC is difficult to be graphitized and is typically produced from a precursor with a strong cross-linked structure. The distinctive "pseudo graphite"[36] HC structure featured by disordered nanostructure with turbostratic nanodomains increases the structural stability by adding extra rigidity and buffer room to prevent volume expansion. The larger (002) peaks, increased interlayer spacing, and smaller grains that are provided by this disordered structure in the c-direction assist in preserving the structural integrity of materials[37]. Additionally, HC has a high standard potential of K^+/K, which helps to prevent the growth of potassium dendrites and enhance safety.

There is no denying that SIBs are developing quickly, and several HC materials have been presented with distinctive structures and outstanding performance. In 2016, Jian *et al.* successfully added HC microspheres (HCS) to KIBs for the first time by pyrolyzing the hydrothermally treated sucrose[38]. With remarkable long-term stability, the typical HCS voltage curves showed a sloping form in the high potential area and a quasi-plateau region in the low potential area. In 2018, He *et al.* created highly disordered HC from degreased cotton, which displayed high initial coulomb efficiency (73%)[39]. This explains the resultant distinctive porous structure, huge specific surface area, and extremely high electrochemical performance of the disordered HC[40].

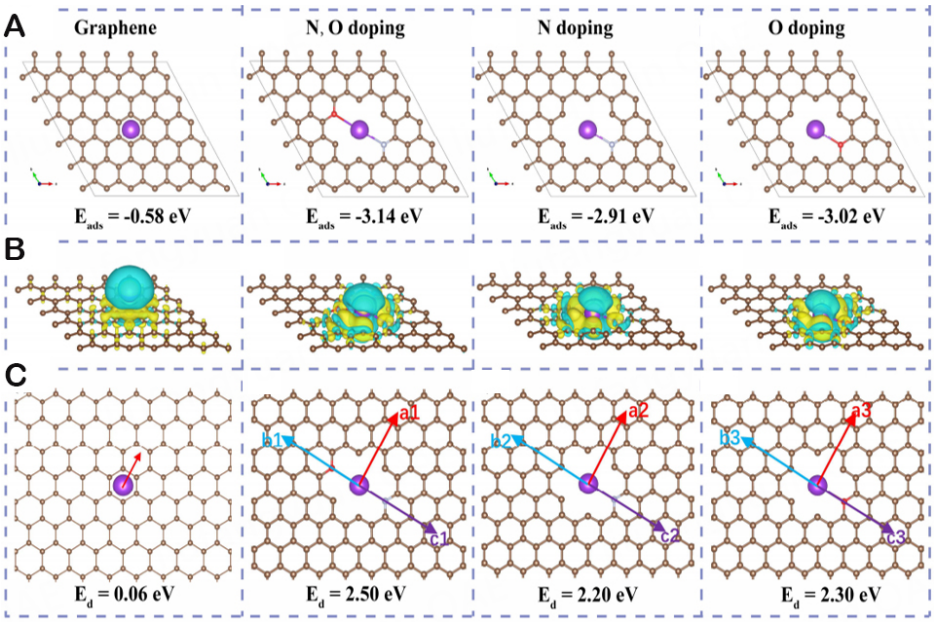

Figure 4. Theoretical simulations of K atom adsorption and diffusion in different structures. (A) Top view of K^+ adsorbed in graphene, along with N, O doping; N doping and O doping structures, and the related adsorption energies. (B) The corresponding side view of the electron density changes of the K atom adsorbed on these structures, and yellow and blue spots represent raised and reduced electron densities, respectively. (C) Top view of the structures with K atom diffusion and associated diffusion energies. The atoms C, N, O, and K are represented by the brown, silver, red, and purple balls, respectively. Copyright 2020, Nano Energy. Theoretical simulations of K adsorption in different structures[11].

Furthermore, the electrochemical energy storage mechanism of HC as KIB anode material has been widely discussed. The unique structure of HC at the molecular level provides many active sites for the storage of Na^+/K^+, which makes its real capacity limit as an electrode material immeasurable. Based on this, different storage mechanisms have emerged. In 2000, the "insertion absorption" concept, additionally referred to as the "house of cards model," was initially reported by Stevens *et al.* after they researched the storage mechanism of Na^+ in nanoporous HC[41]. In this model, Na^+ can be inserted into the interlayer of carbon microdomains at high potential and filled with pores at low potential. Since then, a lot of research has been conducted on the Na^+ storage mechanism. Kim *et al.* developed HC with two distinct crystallinities as anode materials for SIBs[42]. Microcrystalline cellulose (MCC) with more micropores formed by removing amorphous regions exhibits higher specific capacity (300 mAh/g) and rate performance. The impact of amorphous pore structure on the reversible storage ability of sodium was then further investigated on the basis of Na MAS NMR analysis, as shown in Figure 5A. The Na ions can be stored more efficiently in the nanopores created by larger and more open pores, which also increases the pace at which ions diffuse. In 2015, Bommier *et al.* proposed a novel Na^+ storage mechanism: the "intercalation filling" mechanism [Figure 5B][43]. In the platform area, Na^+ is filled into the nanopores in addition to being embedded in the graphite layer and adsorbed in the defective carbon materials in the slope area.

Recently, the adsorption mechanism in the high potential zone and the embedding mechanism in the low potential region were the two separate K^+ storage mechanisms that Li *et al.* discovered in porous HC (p-HC)[44]. Among this, a sufficient number of them serve as an ion trap and ion buffer reservoir in the porous structure, which improves K^+ storage and reduces volume expansion. Similar results were also obtained by Wu *et al.* in their study on the synthesis of luffa-derived pseudo-graphite (LPG) through alkali treatment and one-step pyrolysis[45]. The K^+ storage mechanism of KIBs is primarily responsible for their strong performance. As shown in Figure 5C, the slope area during the initial discharge process (Li^+ is

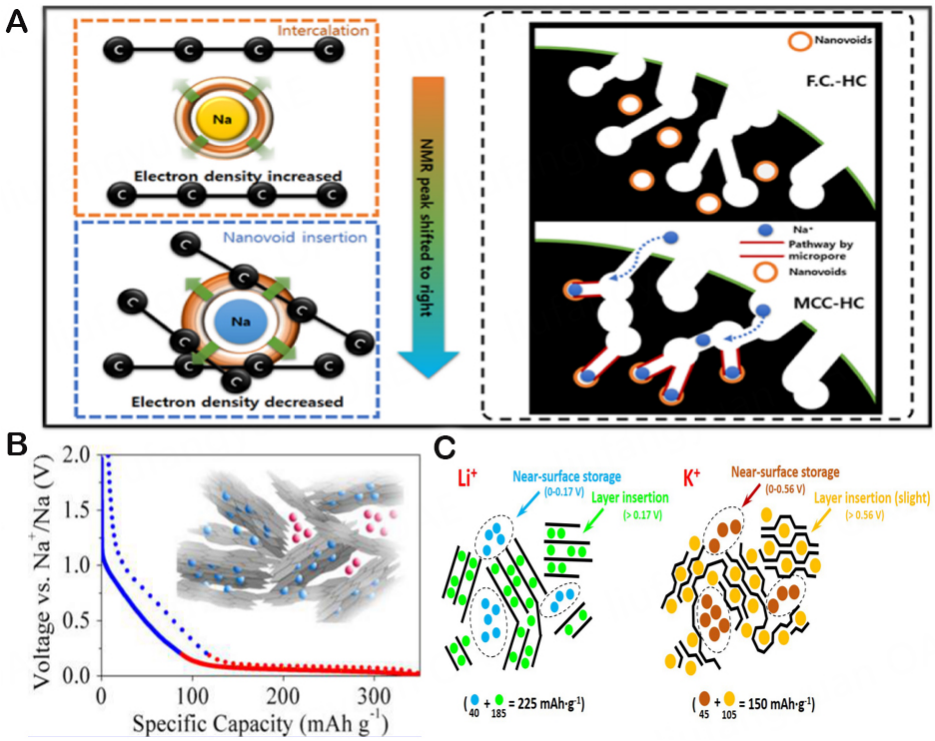

Figure 5. (A) Schematic diagram of the adsorption and pore filling mechanism of sodium ions in nanopores based on NMR analysis. Copyright 2021, The Journal of Physical Chemistry C[42]. (B) Visualization of the "intercalation pore filling mechanism" of sodium ion storage in HC. Copyright 2015, American Chemical Society[43]. (C) Ion storage mechanisms of Li^+ and K^+ in LPG materials. Copyright 2019, Electrochimica Acta[45].

0-0.17 V; K^+ is 0-0.56 V) is linked to the adsorption of alkali metal ions in the near-surface area of HC activated by heteroatoms and various defects, and the platform area during the subsequent discharge process (Li^+ is 0.17-3 V; K^+ is 0.56-3 V) is traced back to the ion insertion into the graphite layer and the formation of ACx (A = alkali metal ions, LiC_6 and KC_8). However, K ions are thought to be more challenging to enter into layered graphite due to the differing atomic radius.

To further interpret the K-storage mechanism in HC, Yuan *et al.* has successfully created a number of chemically active HC spheres (AHCS) with adjustable micro/mesoporous structures to investigate the connection between K migration behavior and micro/mesoporous structure[46]. They also revealed that the storage mechanism of K ions in the HC system can be divided into two stages: adsorption and embedding. There is still much to learn about the fundamental K^+ storage process in HCs and the internal factors impacting K^+ storage behavior, despite the fact that research on HC materials as KIB anodes has advanced greatly over the years.

Due to its inherent characteristics, HC provides good bearing capacity and structural integrity[47]. Among them, Bin *et al.* prepared functional porous hollow carbon materials using molecular/environmental variable-controlled growth processes [Figure 6A][48]. And their extremely low density and low ICE, which results in a low bulk density, restrict their usefulness. In order to overcome the poor diffusion dynamics in KIBs, Chen *et al.* developed a graded N-doped HC microsphere (NCS) composite material with high porosity[49]. The unique porous structure provides more buffer space for volume expansion in the electrochemical process [Figure 6B]. The charge distribution was examined, as shown in Figure 6C-E, in order to systematically analyze the impact of N doping on the K^+ storage performance in NCS materials.

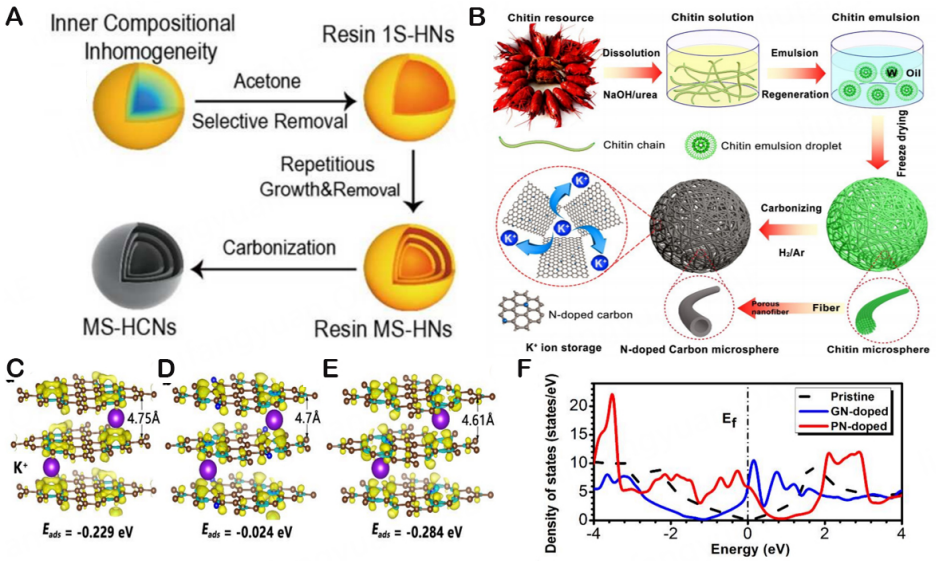

Figure 6. (A) Schematic illustration of the different shape evolution paths for hollow structures. Grey, yellow, and blue represent carbon, insoluble component, and dissolvable component, respectively. Copyright 2017, Journal of the American Chemical Society[48]. (B) Schematic illustration for the large-scale fabrication of hierarchically porous nitrogen-doped carbon microspheres. (C-E) The electronic density differences of K^+ ion adsorbed on pristine carbon, GN-doped carbon, and PN-doped carbon, respectively. (F) The density of states of corresponding carbon materials. Copyright 2017, Energy Storage Materials[49].

The nearly full transfer of Valence electron density from the carbon atom to K^+ demonstrates its ionic characteristics. Among them, the density of states (DOS) diagram in Figure 6F shows that more electrons in the carbon materials doped with graphitic N (GN) and pyridinic N (PN) are conducive to improving the DOS value at the Fermi level (EF), thereby increasing the electronic conductivity. Controlling the microstructure of HC (interlayer, defect, heteroatom doping) is thought to be a successful method for enhancing K^+ storage performance. Zhang *et al.* successfully prepared N-doped CoSe/C composite materials with egg yolk-shell structure, as shown in Figure 7A[50]. CoSe nanoparticles are completely surrounded by a carbon skeleton with high N content and graphitization degree, exhibiting high capacity and excellent rate performance. Lu *et al.* prepared porous N-doped CNF aerogel from chitin as the anode material of SIBs, which shows a high reversible capacity of 282 mAh/g at 0.1 A/g and excellent cycle stability[51]. DFT calculations were used to investigate the effect of N-doped on the electrochemical performance of SIB anodes. Figure 7B shows different types of N-doped graphene groups and high electron density regions, mainly including defect pyridine-N (N-6), defect N-6, pyrrole-N (N-5), and large defect (pyridine/pyrrole/graphite-N) (N6-N5-NG). Among them, the binding energy of Na^+ adsorption on the corresponding structure is -0.89 eV, -0.94 eV, and -1.67 eV, respectively, and the distance between Na^+ and the surface of graphene sheet is 2.05 Å, 0.99 Å, and 0.89 Å [Figure 7C], respectively, indicating that the N6-N5-NG-1 structure has a higher electronic conductivity, which is more conducive to the rapid (de-)insertion of Na^+. In summary, the synergistic effect of N doping and defects provides a theoretical basis for the sodium storage performance of porous CNFs.

Attributed to the introduction of N doping has a favorable impact on the Na ion absorption and diffusion, Gao *et al.* further produced a novel KBT-7 electrode with exceptional electrochemical performance from kitchen biological waste of 700 °C carbonized waste black tea by layered porous structure and co-doping effect[52]. The impact of defects and N, P co-doping on the kinetics of K adsorption capability was further explained using DFT analysis. The differential charge density distribution and adsorption energies of the systems with and without the carbon defect, the carbon defect, the N-doped NC_3 (graphite N), the NC_2

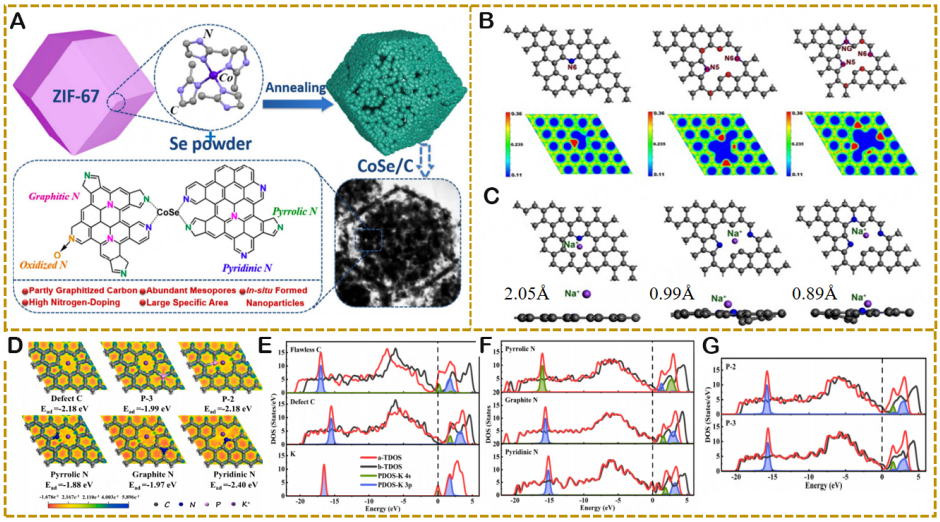

Figure 7. (A) Schematic illustration of the preparation of the nitrogen-doped CoSe/C composites. Copyright 2017, ACS Applied Materials and Interfaces[50]. (B) The DFT optimized structure of N6, N6-N5-1, and N6-N5-NG-1 N-doped graphene and the corresponding electron density. The blue and red regions correspond to the electron-rich and electron-deficient regions, respectively. (C) Optimized top and side views of Na^+ adsorption on corresponding structures. Copyright 2019, Applied Surface Science[51]. Top views of the K-absorption models (D) of defect C, P-3, P-2, pyrrolic N, graphite N, and pyridinic N frameworks, the Ead, and the differential charge density distribution maps. (E-G) The TDOS and the PDOS before and after K adsorption. Copyright 2021, Applied Surface Science[52].

(pyrrole N and pyridine N), the P-doped PC_3 (P-3) and the P-doped PC_2 (P-2), are each shown in Figure 7D. The charge transfer between the K atom and the carbon-based framework is what causes the charge density at C to fall when the K atom is absorbed by the surface, and electrons gather on the carbon atom nearby. Additionally, the variation in charge densities at various sites following K adsorption suggests that the inclusion of N, P doping or defects will dramatically increase the adsorption energy of the structure and intensify the electron transfer event. Figure 7E and F displays the total density of states (TDOS) before and after K adsorption for the systems with defect C, defect C, P-3, P-2, pyrrole N, graphite N, and pyridine N (designated as a-TDOS and b-TDOS, respectively), as well as the corresponding partial density of states (PDOS) of K 4s and K 3p in the K adsorption model. By comparing the TDOS before and after K adsorption, it can be shown that the addition of K^+ will trigger the DOS value guide band at the EF to shift in a certain direction, increasing the relative electronic conductivity, which is mostly caused by the contribution of K atomic orbital. The pyridine N model also exhibits the largest TDOS at the EF, which is further subdivided into two peaks, as seen in Figure 7F and G. The findings demonstrate that the sample with a moderate amount of pyridine nitrogen has improved conductivity when compared to other heteroatom doping models. Different N doping strategies can provide different electrochemical properties for HC materials. Thus, Yang *et al.* created a hollow biomass carbon sphere (NOP-PB), where N/O/P ternary doping increased the interlayer distance on the graphite surface and added more defect sites[4]. The special solid hollow porous structure can buffer the volume expansion of the potassium insertion process, promote the charge transfer of K ions and electrons, and greatly improve the electrochemical performance of the material. The adsorption and diffusion mechanism of K^+ in HC and NOP-PB electrodes can be better understood by simulating the effects of N, O, and P doping on K^+ adsorption behavior via DFT simulations. N-5 and P/O doping are the most effective at enhancing the electronic conductivity of electrode materials, according to a number of calculations and analyses. As a result, NOP-PB electrodes perform better in terms of potassium storage.

HC exhibits good speed capabilities and excellent structural integrity owing to its loose structure[53]. It should be underlined that HC produced during pyrolysis always performs poorly for K ion storage in carbon-based materials. Their extremely low density and low ICE result in low bulk density, limiting their usefulness. As a result, designing a carbon-based anode with a decent degree of graphitization, a finely tuned pore structure, and a chosen surface function is extremely optimal. Surprisingly, not as many individuals are aware of how the solid electrolyte interface (SEI) film impacts the electrode reactivity and changes during the cycle. The commercialization of HC as a high-performance KIB anode will be greatly influenced by this.

Nanoporous carbon composite anode for KIBs

Compared with traditional carbon materials, nanoscale carbon-based materials with high conductivity and specific surface area, such as carbon nanotubes (CNTs), carbon nanospheres, and CNFs[54], can store more charges at the interface and improve the specific capacity and rate performance of KIBs[55,56]. Due to the restrictive C@C, It has incredible elasticity, which increases its mechanical properties of strength, stiffness, and durability[57]. CNTs become one of the most viable carbon materials among potential KIB anodes because of their inherent mechanical properties and connected conductive network, which makes them become a crucial part in sustaining electrode integrity during the (de-)potassium process for alkali metal ion batteries[58]. The cautious alteration of the shape and size of nanoscale carbon materials is a rational and efficient modification method since nanomaterials with various geometric configurations can enhance the ion storage performance of electrode materials to diverse degrees. Given its established use in LIBs, some typical examples of success may be applied to KIBs. In 2017, freestanding porous CNF paper was used as an anode for KIBs by Zhao *et al.*, which showed excellent reversible capacity (211 mAh/g after 1,200 cycles at 0.2 A/g) and rate performance[59]. As said by Cao *et al.*, a carbon nanocage (CNC) can greatly lessen anisotropy and, as a result, prevent layer slippage[60]. Based on their distinctive cage structure, CNCs have outstanding discharge capacity and capacity retention as an anode material for KIBs.

Numerous modification techniques of carbon fiber materials have been documented in an effort to further enhance the efficacy of K ion storage in CNFs. High-performance KIBs utilized unique anodes made by Wang *et al.*, which consisted of highly active hollow carbon nanosphere composite materials (AHCS) with large interlayer spacing, high specific surface area, and surface oxygen-containing functional groups (OCFGs)[61]. The introduction of OCFGs further improves the pseudo-capacitive behavior and specific capacity. After chemical activation, the interlayer gap (0.408 nm) of AHCS is significantly larger than that of hollow carbon nanospheres (HCSs), which can accommodate more reversible K^+ insertion and removal to adapt to larger volume expansion during the (de-)potassium process. Moreover, OCFGs offer additional active sites, which can increase the capacity of reversible K storing. As the anode of the KIB, AHCS exhibits exceptional initial specific capacity, ultra-long cycle life, and extraordinary magnification performance as a result of the synergistic impact of structural properties. The interlayer spacing, surface oxygen functionalization, and layered porosity of carbon-based anodes are highlighted in this investigation as crucial factors in potassium storage. Furthermore, Figure 8A illustrates the porous carbon fibers (PCFs) that Sun *et al.* created utilizing the electrospinning technique as independent electrode materials for high K ion storage[62]. These PCFs have a high reversible capacity of 256 mAh/g under circumstances of 50 mA/g. Corresponding to the potassium storage process [Figure 8B], larger holes increase the surface area, enabling PCFs to absorb and hold more K^+. Therefore, the synergistic effect of K embedding and K clustering is responsible for the extremely reversible potassium storage performance. And Wu *et al.* further fabricated macroporous honeycomb CNFs (MHCNFs), where poly(tetrafluoroethylene) emulsion (PTFE) is primarily involved in the creation of porous materials[63]. Extremely high potassium storage capacity and competitive rate capacity are displayed by the adhesive-free electrode [Figure 8C]. Additionally, a porous structure can offer enough gaps to offset a significant volume shift while attaining prolonged cycling stability[64,65]. Besides,

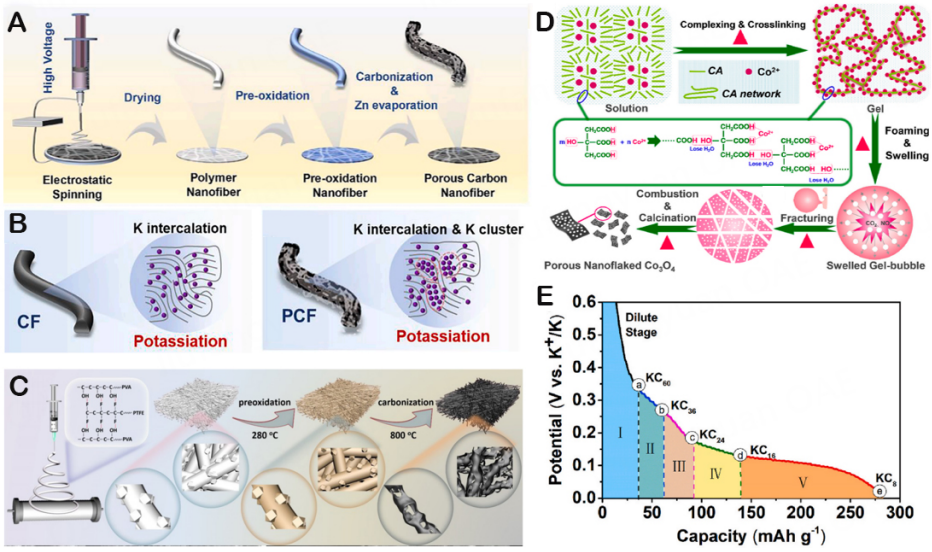

Figure 8. (A) Schematic illustration of the synthesis process of PCF. (B) schematic of K-ion storage mechanism for CF and PCF. Copyright 2022, Chemical Engineering Journal[62]. (C) Schematic illustration of the synthesis process of MHCNFs. Copyright 2021, ACS Applied Materials & Interfaces[63]. (D) Schematic presentation of proposed growth mechanism of porous nanoflaked Co_3O_4. Copyright 2020, Journal of Power Sources[66]. (E) The discharge curve (solid line) of the third cycle of HG-CNFs and the theoretical capacity contribution of each K-GIC transition reaction marked by dotted lines. Copyright 2020, Journal of Power Sources[67].

Wen *et al.* prepared PNF-Co_3O_4 as a KIB anode via a solutions-combustion process and proposed a "bubble gum fracture effect" as its main growth mechanism [Figure 8D][66]. The excellent electrochemical performance of PNF-Co_3O_4 is mainly attributed to the fact that the lower discharge platform (0.3 V) can generate a higher working voltage while having the discharge platform slightly higher than the potassium plating potential can partially reduce the formation of dendrites and improve the safety. Compared with bulk materials, porous structures can withstand larger volume changes and shorten the diffusion path of K^+, thus improving electrochemical performance. These findings provide a better understanding of the electrochemical Li storage behavior of PNF-Co_3O_4. In 2020, highly graphitized CNFs (HG-CNFs) were created by Tian *et al.* by electrospinning, preoxidation, and carbonization[67]. As seen in Figure 8E, the discharge voltage distribution of the third cycle of HG-CNFs exhibits several platforms in the low potential area, indicating a phase shift in the K-GIC system. The potential distribution exhibits a consistent phase shift from KC_{60}, KC_{36}, KC_{24}, and KC_{16} to KC_8 in the dilution stage, in accordance with the trend of voltage decrease. HG-CNFs electrodes may gain high energy density, high reversible capacity (200 mAh/g), and stable structure owing to the independent fiber network and highly graphitized structure. In 2022, Zhao *et al.* prepared KIBs with significant K ion storage performance by porous CNFs, including excellent reversible specific capacity(270 mAh/g) and ion mobility[59]. The exceptional performance is attributable to the distinctive structure of CNFs, where the porous design may successfully reduce the volume expansion brought on by the injection of massive K ions.

Several modification strategies have been constructed so as to utilize nanocarbon materials as an alternative alkaline metal ion insertion, adsorption, and diffusion electrode material. Doping heteroatoms [N, O, sulfur (S), P, *etc.*] in nano carbon materials have also been shown to be a successful method to enhance the efficacy of K ion storage for the following reasons: (1) Heteroatom doping technology can accumulate charges by altering the local electronic structure on the surface of carbon lattice, thereby raising the electronic conductivity of carbon nanomaterials[68]; (2) Heteroatom doping can provide a large number of active sites for K^+ adsorption[69] and; (3) Due to the large covalent radius of nano carbon materials, heteroatom doping

can regulate its interlayer distance[70]. The carbon source generally originates from polyacrylonitrile (PAN) carrying N element, which is the most frequent doped element in CNFs. Thereby N-doped CNFs are often synthesized *in situ* during carbonization. It has been demonstrated that adding more defects due to N doping increases reactivity and that adding better local electronic configurations due to N doping increases electronic conductivity[71]. In 2019, as separate anodes for high-performance potassium-based dual-ion batteries (KDIBs), Zhang *et al.* created graded porous N-doped carbon fibers (HPNCF) with distinct hierarchical architectures (micro, medium, large pores, and nanochannels)[72]. The distinctive structure offers the HPNCF not only an excellent ion transport channel and an intrinsic electronic channel but also adequate buffer space to survive the volume shift of the cycle, which favors enhancing electrochemical efficiency. Moreover, calculations based on the DFT theory are commonly used to examine how N-doped porous carbon materials affect the performance of potassium storage. Through a single carbonization of N-rich energetic metal-organic frameworks (EMOFs), Tong *et al.* created N-doped porous carbon frameworks (NPCF) with a large N content (MET-6)[73]. The greater porosity and specific surface area are responsible for the optimized potassium storage ability (327 mAh/g). To further research the effect of pyrrole and pyridine N-doped porous carbon structures on the K^+ adsorption mechanism, the K ion adsorption abilities and the relative adsorption energy (ΔE_a) at three different models were constructed and calculated by DFT, including pristine C-doping, graphitic N-doping, pyrrolic N-doping. It is evident that the endothermic reaction occurs in the graphite N and C co-doped system, and the extremely unstable potassium insertion reaction may be a result of the electronic abundance of graphite N doping[71]. Whereas, the adsorption energy of pyrrole N-doped C and pyridine N-doped C is much higher than that of the original C, which demonstrates why the K adsorption abilities and specific capacity are made possible by the pyrrolic and pyridinic N-doping. These findings show that improving the kinetics and, consequently, the electrochemical performance of KIBs through the doping of pyrrolic and pyridinic N are effective techniques. Chen *et al.* also prepared a KIB cathode material with a multi-stage structure (N-doped cluster composite hollow carbon fiber) and high reversible capacity (NHCF@NCC), which can effectively reduce the distance that K ions must diffuse before coming into contact with the electrode material[74]. More reactive sites can also be provided by asymmetric N-doped clusters attached to hollow carbon fibers. Benefiting from its high aspect ratio, NHCF@NCC additionally enhances its electrochemical performance as a KIB anode, which can create a self-supporting structure with a three-dimensional (3D) connected conducting network. In order to obtain higher reversible potassium storage capacity and outstanding multiplying performance, Zhao *et al.* produced N-doped sea-urchin-structured porous carbon (N-SPC) with a porous siphon effect and increased kinetics and effectively incorporated it into KIBs, taking cues from the framework of sea urchins and their ability to transfer and absorb K^+[75]. Large specific surface areas, hierarchical micro/mesopores, moderate N-doped defect sites, and appropriate K^+ diffusion barrier energy are all factors of the biomimetic N-SPC that help it achieve amazing cyclability (296 mAh/g at 1 A/g after 2,000 cycles) and rate performance (116 mAh/g at 20 A/g) for KIBs. Moreover, the adsorption energy and DOS of different defect structures were calculated by DFT to investigate the relationship between the adsorption/diffusion behavior of K^+ and N-doped carbon. Previous research[4] indicates that the porous structure is more favorable to the adsorption energy of K^+ than that of the dense structure; thus, diverse N-doping is used for atomic doping in the porous graphene layer, including quaternary-N (N-Q), N-5, and N-6. The lowest adsorption energy (-4.40 eV) reveals that K^+ is significantly easier to absorb by N-6 than N-Q or N-5, resulting in a significantly higher reversible capacity and superior rate performance [Figure 9A]. As a result, several N-6 dosages were used to compute the change in K^+ storage with various N-doping contents. The adsorption energy rises as the concentration of N-6 climbs, as seen in Figure 9B. Unexpectedly, the DOS of the associated carbon structure exhibits the same pattern. The addition of more N-6 doped graphene layers demonstrates an improved DOS around the EF in comparison to a single N-6 doped, leading to increased electrical conductivity [Figure 9C]. But as the amount of N doping grows, the barrier energy (E) for K^+ diffusion likewise rises (from 3.67 eV to 3.86 eV and 4.10 eV), showing that the migration energy needed for

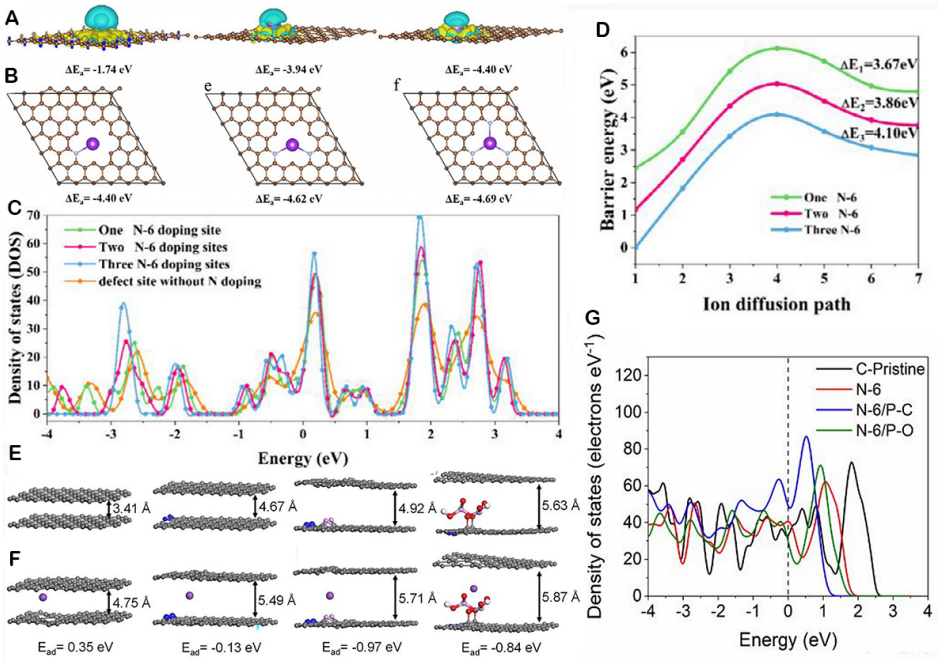

Figure 9. (A) Top view of a single K atom absorbed in quaternary-N (N-Q), pyrrolic-N (N-5), and pyridinic-N (N-6). (B) The adsorption energy of different amounts of one N-6, two N-6, and three N-6. (C) The DOS of the defect site without N-doping, one, two, and three N-6 doping sites. (D) The barrier energy of one N-6, two N-6, and three N-6 doping sites. Copyright 2021, Electrochimica Acta[75]. (E) The interlayer distances of different carbon structures before insertion of K^+: pristine carbon, N-6 doped carbon, N-6/P-C co-doped carbon, and N-6/P-O co-doped carbon. (F) The layer spacing and adsorption energy of K^+adsorbed by corresponding structures. (G) The DOS of different carbon structures. Copyright 2020, ACS Nano[76].

K^+ diffusion doubles [Figure 9D]. In order to further develop and build enhanced KIB anodes, it is, therefore, possible to demonstrate the largest tilt capacity and quick K^+ diffusion capacity using optimized N-SPC materials with more K^+ adsorption sites and smaller K^+ diffusion barriers.

Due to the extensive study that has been done on the diatomic co-doping modification technology in CNFs, it is anticipated that high-performance CNF anodes will be produced thanks to the synergistic interaction of two distinct heteroatoms. In 2019, Ma *et al.* created sodium polyacrylate as the carbon precursor for graded N, S co-doped porous carbon (NSPC)[68]. The structure of nitro and S co-3D doping makes it easier to inject K ions, increases layer gap, and hence enhances electronic conductivity. NSPC has exceptionally high reversible capacity (289.7 mAh/g after 70 cycles at 50 mA/g) and outstanding cycling performance as the anode material for KIBs. Besides, several studies showed that the introduction of P improved the electrochemical performance of the carbon anode of KIBs. Thus, Gong *et al.* successfully constructed an independent P/N co-doped porous carbon monolithic (PN-PCM) anode for KIBs using supercritical CO_2 foaming technology and a number of pretreatment steps to increase the potassium storage capacity (including amidation, phosphorylation, and heat treatment)[76]. The PN-PCM anode has good reversible specific capacity (396 mAh/g at 0.1 A/g after 300 cycles), initial coulomb efficiency (63.6%), and magnification performance owing to the 3D macroporous open structure and the heterodimer of high P/N ratios. According to theoretical calculations, P-C bonds are more useful for enhancing potassium storage and improving carbon conductivity through adsorption in P/N co-doped carbon, whereas P-O bonds are more beneficial for extending the distance between carbon layers and lowering the ion diffusion barrier. Based on this, further research has been done to determine how P-C and P-O functional groups affect the electrochemical performance of P/N co-doped carbon materials (the most typical N-6 bond is used to

represent N doping). The layer spacing of original carbon, N-6 doped carbon, N-6/P-C co-doped carbon, and N-6/P-O co-doped carbon is depicted in Figure 9E. This graph demonstrates how the layer spacing of carbon may be greatly increased by the addition of P, particularly for the P-O form. Additionally, the inclusion of N-6, P-C, and P-O bonds increases the E_{ad} of carbon, as seen by the corresponding adsorption energies (E_{ad}) of each structure following K^+ intercalation [Figure 9F]. N-6/P-C co-doped carbon exhibits a lower value than N-6/P-O co-doped carbon (-0.97 eV), indicating that the P-C bond contributes most to the capacitance of P/N co-doped carbon. Then again, Figure 9G displays the DOS of four carbon structures. N-6/P-C co-doped carbon and N-6/P-O co-doped carbon both exhibit higher DOS around EFs than original carbon and N-6 doped carbon, with N-6/P-C co-doped carbon exhibiting the greatest DOS. Further analysis proved that the addition of P significantly increases the electrical conductivity of carbon and that the P-C bond contributes a greater amount of electron density to the EF than the P-O bond. Therefore, it is thought that carbon with an optimal P-O/P-C ratio will still have great electrochemical performance.

Consequently, N doping is the correct strategy since it may efficiently increase the adsorption energy toward K^+ ions[77]. To achieve high magnification capacity, the creation of KIBs will also need appropriate nanocarbon materials[78,79]. The design of nanostructures is typically accompanied by an increase in the conductivity of the material, which can significantly shorten the electron transmission path and speed up the diffusion of K^+ in the bulk phase[80,81]. One of the most successful methods for enhancing the electrochemical performance of carbon materials is the production of CNTs, carbon nanowires, and other nanomaterials. The high throughput electrochemical performance may also be directly predicted by DFT calculations, accelerating the screening and practical design of KIBs anode materials. At the same time, it can give us fresh perspectives on how various anode materials behave from a molecular to a macro level. Additionally, it offers new insights into how to create high-performance KIBs.

ALLOY-BASED ANODES FOR KIBS

With the creation of polyanion compounds and layered transition metal oxides on the cathode side, significant advancements have been realized[82,83]. Despite having a high reversible specific capacity of 230 mAh/g, the output voltage of graphite is very close to the potential for the deposition of potassium[84]. Due to their weak conductivity and constrained capacity as a result of their innate characteristics, insertion-type anode materials are unable to meet the demands of high energy density[85]. The conversion anode materials for alkaline ion batteries, such as transition metal oxides, sulfides, and phosphides, have been widely used in the research of high-performance KIBs[86]. Contributed to the relatively high voltage of the platform, the energy density of the entire battery is prone to significant attenuation[87,88]. Apart from that, the highly active metal K tends to generate dendrites during electrochemical charging and discharging, which separates the active component from the collector and drastically decreases capacity[89,90]. As a result, there are still a lot of obstacles to overcome in the invention of anode materials[91].

Nowadays, the high theoretical specific capacity, good conductivity, and appropriate working potential of alloy-based anode materials, such as P[92], tin (Sn)[93], antimony (Sb)[5], bismuth (Bi)[94], Si[95], and Ge[96], and their oxides, sulfides, and selenides, and so on, have recently attracted significant attention to ensure the high energy density and safety of secondary batteries[97]. For instance, the theoretical capacities of Si, Ge, Sn, and Sb for LIBs are high, at 4,200 mAh/g, 1,600 mAh/g, 994 mAh/g, and 660 mAh/g, whereas P and Sn can form alloys with sodium, with theoretical capacities of 2,596 mAh/g and 847 mAh/g, respectively[98]. As a result, it is anticipated that the alloy-based anode employed for high-energy-density KIBs would receive careful consideration. Theoretically, alloy-based anodes made of S, Si, P, Ge, Sn, Sb, and Pb can be alloyed with potassium in a variety of ratios, as determined by Kim *et al.*[99]. Among them, the sulfur electrode has become one of the candidate electrode materials in metal lithium-ion batteries since their affordable and

enormous theoretical capacity[100]. However, the difficult electrochemical reactions between cyclo-S_8 and K^+, such as the reduction from K_2S_3 to K_2S, are extremely challenging, thus excluding it from the field of candidate electrode materials for KIBs. Some studies have shown that reforming the chemical structure of S can effectively improve the electrochemical performance of S and regulate the electrochemical behavior of S[101]. Using this information as a foundation, Tian *et al.* proposed a S-modified doped biomass bamboo charcoal (S-BC) negative electrode material that shows remarkable reversible specific capacity (339.3 mAh/g at 50 mA/g) as a KIB anode material[102]. The remaining O atoms and doped S of the biomass materials render an abundance of active sites for electrode materials, significantly raising the electrical conductivity. However, during the cycle, due to the multi-electron reaction, the deep potassification of the S-based anode material will produce a large volume expansion, and the active material will fall off, resulting in battery failure[103,104]. In addition, the large volume expansion leads to multiple continuous exposures of specific surface areas, which accelerates the loss of active substances and the consumption of electrolytes[105], reduces the coulomb efficiency and overall energy density of the battery, and makes the development of high-capacity electrode materials more difficult. Thus, Yang *et al.* prepared multi-shell hollow nanospheres (ASHCs) with a high content (about 32 wt%) of single-atom S doping[106]. Based on the superior reaction kinetics of single-atom S, ASHCs exhibit upgraded reversible capacity and fantastic rate capability as KIB anode materials. Furthermore, the special nanoporous structure of the carbon-based material may efficiently reduce volume expansion during the electrochemical reaction and guarantee the structural integrity of the substance.

Furthermore, a large number of studies have shown that the creation of nanostructures and internal spaces, heteroatom doping, protective coating, introduction of conductive buffer media, and application of appropriate materials can effectively improve the structural stability of materials and promote fast ion/electron transfer kinetics. For example, Wang *et al.* wrapped CoS nanoparticles in CNFs/CNTs to prepare a special micro/nano multi-scale matrix material[107]. The unique core-shell structure not only prevents the aggregation of CoS in the curing process but also restricts the formation of active nanoparticles, thus improving the structural stability of the materials. In addition, the synergistic effect of abundant active sites of CNFs and their high electrical conductivity greatly improved their reversible capacity (411 mAh/g) and magnification performance as KIB electrode materials. The effective surface modification strategy provides a new idea for developing high-performance electrode materials. Although many effective strategies have been used to prepare high-performance electrode materials, the poor extended cycle life and low coulomb efficiency of alloy-based anode materials still limit their practical application[108]. Therefore, exploring new KIB anode materials to achieve a good combination of capacity, recyclability, and recovery rates remains a top priority.

Sb and its derivative anode for KIBs

With its abundant resources, low price, excellent theoretical capacity (660 mA h/g), and adequate voltage window, Sb has drawn a lot of interest as an alternative anode for Li^+ and Na^+ storage[13]. Then, Han *et al.* described the binary phase diagram of the K-Sb system[10]. The phase diagram demonstrates that Sb will go through a series of potassium alloying transformations, including KSb_2, KSb, and K_5Sb_4, before the development of the K_3Sb phase. The thermodynamic stability of the K-Sb phase can also be investigated using the binary K-Sb phase diagram. In an attempt to shorten the ion diffusion path, 1D nanowires, nanorods, and nanotubes have all been investigated extensively as part of the nano-engineering profile strategy of alloy-based anode materials. As a KIB anode, Yi *et al.* created nanoscale Sb particles with high reversible capacity (381 mAh/g at 100 mA/g) and capacity retention rate (210 mAh/g at 500 mA/g after 200 cycles)[109]. A series of related characterization and *in situ* tests show that the typical peaks of the cubic K_3Sb phase disappear completely after the complete removal of potassium and eventually form amorphous Sb, while the cubic K_3Sb phase forms again after the complete embedding of potassium. It is further proved

that the storage mechanism of potassium is an alloying mechanism. Then, Gabaudan *et al.* explored the K^+ storage mechanism in Bi/K and Sb/k systems, respectively[110]. Figure 10A demonstrates the electrochemical activity of Sb and Bi electrodes in KIBs. At the conclusion of the first discharge, cubic K_3Sb is formed after the kaliation of Sb through the creation of amorphous intermediates, with minimal hexagonal K_3Sb contribution. However, the potassification/depotassification process of Bi first forms crystals K_3Bi_2 and KBi_2 and finally forms hexagonal K_3Bi. The data indicate that the potassium storage mechanism of the two systems in KIBs is an alloying mechanism, and the stability of different phases of electrochemical reaction needs to be further investigated.

Besides, Shi *et al.* successfully prepared 3D flowered antimony oxychloride ($Sb_4O_5Cl_2$) as the anode material of PIBs by a hydrothermal method[111]. As depicted in Figure 10B, the XRD results of $Sb_4O_5Cl_2$ electrodes show that the typical peak of $Sb_4O_5Cl_2$ weakens with the formation of KCl, KSb, and K_3Sb products and reversibly recovers from 0.01 V to the original strength at 3.0 V during (de-)potassification process. The presence of KCl and K-Sb alloys further confirms the synergistic effect of conversion type and alloying reaction. Therefore, the reversible electrochemical mechanism of storing K^+ ions by $Sb_4O_5Cl_2$ can be established: $Sb_4O_5Cl_2 + k^+ + e^- \Leftrightarrow KCl + K_3Sb + K_2O$.

Unfortunately, the unavoidable high volume strain of the cyclic operation causes the rupture of the active material and insufficient electrical contact, which immediately causes a quick attenuation of capacity and prevents the practical use of KIBs[112]. Thus, numerous modification methods have been developed till now with a view of balancing the (de-)alloying process of Sb-based materials, which include nanoparticles[113], the inclusion of carbon components[114], the improvement of adhesives[115], and the creation of open structures[116]. Surprisingly, mixing alloy anodes with carbon materials may dramatically boost their cycling stability. The investigation on the electrochemical behavior of Sb-C composite electrodes as KIB anodes, which deliver 650 mAh/g high reversible capacity and good coulomb efficiency, was initially reported by McCulloch *et al.*[5]. According to in-situ XRD and electrochemical analysis, the discharge result is the final cubic K_3Sb phase. Additionally, SEM inspection at various voltage cut-off points revealed that the Sb-C electrode underwent significant expansion during the potassium alloying event. Therefore, carbonaceous materials are frequently utilized in Sb-based systems as a volume change buffer to conduct ion conduction in the full potassium alloying/dealloying reaction. In the research of Ko *et al.* the multi-component electrode [Sb-C-rGO (reduced graphene oxide)] with uniform and fine Sb particles was prepared from Sb-based composite materials containing Sb nanoparticles, amorphous carbon, and rGO [Figure 10C][117]. And the side reactions in potassium metal and the electrolyte, not the degradation of Sb nanoparticles, are to blame for the capacity decline in the Sb-C-rGO cell. And three intermediate phases, $K_{0.5}Sb$, $K_{1.0}Sb$, and $K_{1.25}Sb$, which are congruent with the experimental phase diagram of the K-Sb system, exist between the two reaction end members (Sb and K_3Sb). Among the stable phases, cubic and hexagonal K_3Sb polycrystalline phases are more stable than other crystalline phases. As can be shown in Figure 10D, the two polymorphic forms of K_3Sb are structurally identical. The hexagonal system (h-K_3Sb) is more stable than the cubic system between the two polymorphs [Figure 10E]. The relative stability of K_3Sb polymorphs is the same at a higher theoretical calculation level. This finding demonstrates that the electrochemically produced phase of c-K_3Sb is metastable. One intriguing aspect is the ability of the final phase, the c-K_3Sb phase, to change into a stable h-K_3Sb phase after forming. However, no phase change was noticed while the battery was in use, indicating that dynamics are hampered during the phase transition from c-K_3Sb to h-K_3Sb. This cubic to hexagonal phase shift may necessitate both the vertical migration of K and the lateral sliding of the K-Sb layer. In actuality, the c-K_3Sb before h-K_3Sb creation is still present. After several hours of heating at the samples between 160 °C and 170 °C, the resultant c-K_3Sb can likewise be changed into h-K_3Sb. According to the aforementioned findings, the c-K_3Sb to the h-K_3Sb phase transition is dynamically non-spontaneous under

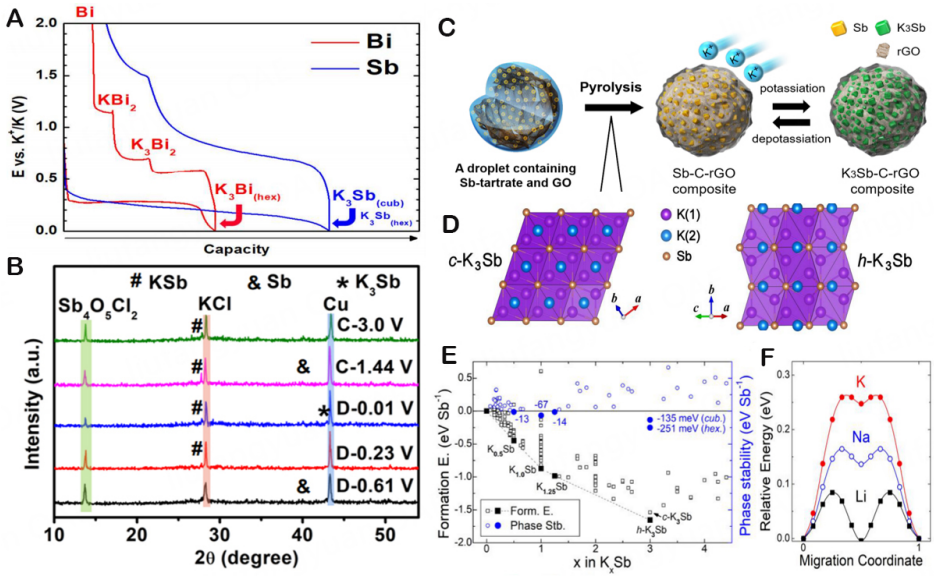

Figure 10. (A) Schematic diagram of potassium mechanism of Bi/K and Sb/k systems in KIBs. Copyright 2018, The Journal of Physical Chemistry C[110]. (B) The XRD patterns for electrodes at various charge/discharge states. Copyright 2022, Applied Surface Science[111]. (C) Schematic presentation of the formation and (de-)potassiation process of Sb-C-rGO composite. (D) Crystal structure of cubic K_3Sb (c-K_3Sb) and hexagonal K_3Sb (h-K_3Sb). (E) Formation energies of KxSb obtained by the ionic substitution method. Phase stability is a relative energy of a given phase compared to all other materials with different compositions. (F) Atomic migration barriers in the cubic A_3Sb phase (A = K, Na, and Li). Copyright 2019, ACS Applied Materials & Interfaces[117].

environmental conditions, and the h-K_3Sb phase is more stable. The migration potential barrier of each component atom can be a suitable signal to estimate the phase transition kinetics since the phase transition necessitates the reorganization of atoms. The migration barriers for Li, Na, and K in each cubic A_3Sb phase are 0.09 eV, 0.16 eV, and 0.26 eV, respectively, as shown in Figure 10F. The occurrence of the metastable phase in the K-Sb system and its simple nucleation properties are explained by the higher K atom migration barrier. The inclusion of carbon substrates and nanoscale materials still lowers their energy density despite the tremendous progress that has been accomplished thus far; therefore, in-depth modification exploration continues to be the main focus of research. For example, Ge *et al.* employed Sb@CNFs as the alloy anode to investigate the dynamic volume expansion during the charging and discharging process by *in-situ* transmission electron microscopy (TEM) in order to explore the structural changes of carbon-coated conversion anode materials[118]. Studies indicate that Sb@CNF compound materials can successfully buffer the volume growth of Sb nanoparticles during the K ion insertion/extraction process, which enhances the electrochemical performance[90]. Owing to the aforementioned study, porous structures may successfully prevent the accumulation of Sb nanoparticles and respond to the significant volume variations of Sb during charging and discharging while preserving structural stability. The K^+ diffusion distance can also be minimized via porous structures, which also enable ions to transfer charges quickly along 3D skeletal structures.

Sb also displays considerable volume variations during the alloying/dealloying process, similar to other alloy-based anode materials[119]. Severe battery polarization issues can also be caused by the poor K^+ diffusion rate within Sb crystals[120]. To address this concern, Luo *et al.* created a novel form of N-doped carbon hollow nanotube-wrapped Sb nanorod composite (Sb@N-C) via the nanostructure technique[121]. The hollow structure of 1D conductive carbon covering takes advantage of its advanced structural advantages, including the high conductivity brought on by heteroatom doping, and makes room for the superior ion transfer capacity Sb@N-C, which performs electrochemically quite well. In 2018, An *et al.*

reported a novel 3D nanoporous Sb material (NP-Sb) which is created by vacuum distilling the zinc (Zn) atoms out of a commercial Zn-Sb alloy[116]. It is also discovered that altering the Zn-Sb ratio and distillation temperature can change the shape and porosity of NP-Sb materials. As shown in Figure 11A, the unique nanoporous structure can effectively reduce the volume expansion caused by electrochemical cycling, accelerate the diffusion of K^+, and achieve high electrochemical performance. In the same year, by perfecting the crystal structure and ion storage mechanism, Huang *et al.* reported the heterostructure of In_2S_3-Sb_2S_3 formic acid microspheres and enhanced their electrochemical performance[122]. After a series of characterization methods, it is known that when the voltage drops to 0.9 V, the conversion reaction occurs and generates metal Sb, metal In, and sodium sulfide. Strong pseudocapacitive effects can be produced because In_2S_3-Sb_2S_3 is highly reversible during the charging process, and the InSb phase retained in the Sb_2S_3 gap leaves enough room for later conversion and alloy processes. The synergy of In_2S_3 and Sb_2S_3 also maintains the primary structure and improves electronic conductivity throughout the cycle, reducing the likelihood of a devastating collapse brought on by the structural expansion zone. A CNT-coated electrode is also advantageous for enhancing cycle and rate performance. Therefore, a hollow material that was created using the self-template procedure Sb_2Se_3@C microtubules was reported by Yi *et al.*[123]. The type of alloying in the microtubule is conventional, as confirmed through Sb_2Se_3@C electrochemical behavior and *in-situ* Raman spectroscopy. The original electrode exhibits significant Raman signals at 187 cm^{-1} and 253 cm^{-1}, which are closely related to the production of Sb_2Se_3. These peaks gradually diminish and eventually vanish with the discharge. The rapidly growing signals of the newly discovered peaks at 112 cm^{-1}, 148 cm^{-1}, and 250 cm^{-1} are indicative of the formation of hexagonal Sb. Further discharge causes the peaks at 112 cm^{-1} and 250 cm^{-1} to vanish while the peak centered at 148 cm^{-1} shifts left to 145 cm^{-1} and weakly expands, possibly indicating the transition from hexagonal Sb to cubic K_3Sb phase. According to the aforementioned findings, K_2Se is produced during the first stage of the conventional reaction, and K_3Sb is generated during the second stage of the alloying process. Due to mechanical protection and enough reverse space, Sb_2Se_3@C microtubules displayed cycle stability and a reversible capacity of 312.8 mAh/g at 0.1 A/g after 40 cycles. The carbon-supported hollow structure is advantageous for improving potassium storage in light of the aforementioned findings. Additionally, Xiong *et al.* effectively generated composite nanosheet anodes (BiSb@C) by embedding Bi, Sb alloy nanoparticles into porous carbon matrix through freeze-drying and carbonization procedures[124]. The addition of carbon and Bi significantly reduced the stress and strain brought on by the volume change that occurs during charging and discharging, and as a result, the electrochemical performance was outstanding. The XRD technique was used to properly study the potassium storage mechanism of BiSb@C for further discussion [Figure 11B]. The Bi and Sb phase peaks gradually vanished during the first discharge, and a new peak, K_3Bi and K_3Sb, formed at 0.2 V, indicating that (Bi,Sb) had interacted with potassium to generate K_3(Bi,Sb), respectively. Peaks are seen at 0.7 V during the charging process, indexed to K(Bi,Sb), an intermediate phase during the transition from K_3(Bi,Sb) to (Bi,Sb). In contrast to the first discharging process, the second discharging process yields first K(Bi,Sb) and subsequently K_3 from the potassiation reaction of (Bi,Sb). The identical two-step dealloying process as in the first cycle, K_3(Bi,Sb)- K(Bi,Sb)- (Bi,Sb), is seen in the subsequent charging, indicating a reversible potassium reaction. According to the aforementioned research, the BiSb@C composite materials initially experience an irreversible potassium reaction in the (Bi,Sb)-K_3(Bi,Sb) discharge process, which is then followed by a reversible K^+ (de-)intercalation reaction of K_3(Bi,Sb)-K(Bi,Sb)-(Bi,Sb) [Figure 11C]. These findings demonstrate that the potassization/depotassization process of the BiSb alloy is comparable to that of metallic Bi and Sb. The Bi and Sb in the BiSb@C alloy composite share similar physical physiochemical characteristics and miscibility. This coincident process may help reduce volumetric expansion and improve cycling stability. Moreover, by using a solvothermal reaction and calcination, Wang *et al.* created self-assembled Sb_2S_3 nanoflowers on the surface of an MXene (Ti_3C_2) sheet [Figure 11D][125]. The highly conductive two-dimensional (2D) Ti_3C_2 soft substrate can effectively buffer the volume growth of Sb_2S_3 while simultaneously promoting charge transport dynamics. Additionally, the structural stability of Sb_2S_3

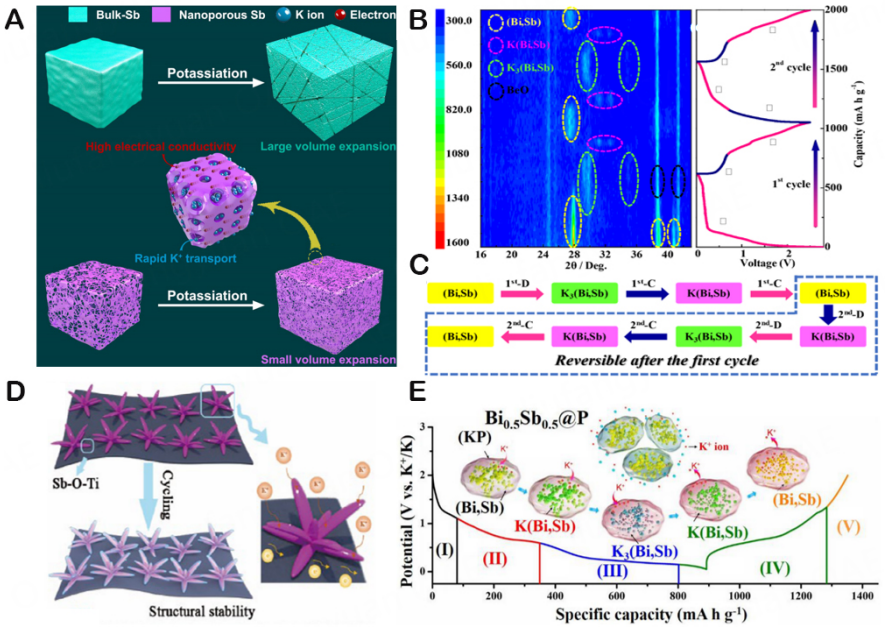

Figure 11. (A) Schematic of potassiation process for bulk-Sb and NP-Sb anodes. Copyright 2018, ACS Nano[116]. (B) XRD diagram of the first two cycles for BiSb@C composite anode. The corresponding CV curve (10 mA/g) is shown on the right. (C) Schematic diagram of potassium/dipotassium process of BiSb@C composite anode. Copyright 2019, ACS Nano[124]. (D) Schematic illustration of Ti_3C_2-Sb_2S_3 during cycling. Copyright 2020, ACS Applied Materials & Interfaces[125]. (E) Schematic illustration of the potassium storage mechanism for the *in situ* XRD results. Copyright 2020, ACS Nano[94].

nanoflowers is improved by their *in situ* growth on the Ti_3C_2 sheet due to strong interface interaction. As a consequence, improving the capacity utilization of KIBs for potassium storage by modifying the binding structure of electrodes is thought to be one of the most adept modification tactics.

What is more, following previous research, double heteroatom doping is a common modification method for Sb-based compounds, which improves their electrical activity. Han *et al.* employed a method of co-encapsulating N and P in carbon nanorods (Sb@NPMC) to create a unique Sb nanoparticle anode material[6]. Due to the collaborative impact of N/P co-doping, SSb@NPMC possesses excellent electrochemical reactivity and electrical conductivity as an anode electrode. Through coordination and spatial co-refinement methodology, Yi *et al.* successfully rGO matrix (SbSA/C) based on S-rich amorphous carbon covering to get highly loaded and well-dispersed Sb atoms[126]. The rGO substrate can be utilized to load atomically distributed Sb species, and the pyrolytic Sb chelate can be used to coordinate certain heteroatoms (S, O) owing to the open 2D space framework. Also, the special preparation method can minimize migration and agglomeration during the electrochemical potassium storage cycle. In fact, the K ion diffusion barrier was dramatically lowered, as demonstrated by DFT calculations and electrochemical analysis. Given the active Sb centers and coordination heteroatoms, SbSA/C electrodes provide excellent rate capability and lengthy duration capability for KIBs. In 2020, an ultra-small Bi, Sb nanocrystalline material (Bi_xSb_{1-x}@P) was synthesized, as reported by Chen *et al.* Bi_xSb_{1-x} nanocrystals with the greatest performance can be obtained through careful management of the ratio of Bi/Sb reactants, which can effectively reduce volume change and electrode collapse during the cycle[94]. Likewise, the P matrix can carry out quick charging and discharging processes because it is a suitable medium for electron and K^+ ion transmission. As shown in Figure 11E, the *in situ* XRD analysis applied to further explain the potassium storage mechanism following K^+ ion insertion and extraction indicates that the chemical pathway: (Bi,Sb) ↔ K(Bi,Sb) ↔ K3(Bi,Sb) is reversible (Bi,Sb). In conclusion, the optimized composition of

$Bi_{0.5}Sb_{0.5}$@P composite electrodes demonstrated outstanding electrochemical performance as KIB anodes. Following the aforementioned findings, Bi_xSb_{1-x}@P nanocomposite materials can improve the potassium reaction with K^+ ions. These physical design techniques wide up a new avenue for the study of Sb-based anode materials in light of the electrochemical properties mentioned above.

Nevertheless, certain theories and experiments have confirmed that stable rare earth-free MnBi materials can generate a ferromagnetic low-temperature phase employing Sb dopant. Thereby, Nguyen *et al.* adopted DFT theoretical calculations to carry out phonon dispersion and DOS analysis of the doping system in order to further clarify the implications of Sb doping on the structural stability, internal magnetism, and electronic structure of MnBi components[127]. Figure 12A-C displays the phonon dispersion and phonon DOS of MnBi, $MnBi_{0.5}Sb_{0.5}$, and MnSb along the high symmetry direction. This figure demonstrates the instability of the MnBi material, which is indicated by the abundance of imaginary frequencies. The number of imaginary frequencies in the system diminishes when Sb is introduced. The imaginary frequencies in the MnSb system vanish, and the system energy becomes more stable when Sb totally replaces Bi. By lowering the magnetic moment, it is possible to stabilize MnBi while Bi is exchanged by Sb. The calculation of the DOS reveals that doping causes a decline in the DOS at the EF. And hence, to investigate how Sb substitution doping influences the electronic structure of MnBi, DOS calculations of spin and lower spin states are employed, along with calculations of energy band structure, which is shown in Figure 12D. Due to their shared crystal structure and the isomorphism of Bi and Sb, the energy band structures of MnBi and MnSb and the related DOS-s data exhibit the same trend. Subsequently, the energy band structure of doped materials splits along some k-paths, and the band within the energy range is divided into two separate bands [Figure 12E]. Along Γ MK Γ k-path, the dispersion curve of the k-path becomes flatter. In contrast, the dispersion curve along the ALHA k-path is split into a unique double dispersion curve, meaning that there is a linkage between the split band and the s orbital, p orbital, and d orbital of Mn and between the split band and the non-split band. Analysis of the DOS concerning $MnBi_{1-x}Sb_x$ demonstrated that the reduction of DOS through the substitution doping from MnBi to MnSb was another effect on the band structure (see Figure 12F). According to the data, this reduction gradually lowers the magnetic moments of Mn and MnBi1-xSbx in contrast to pure MnBi. The study of PDOS for $MnBi_{0.5}Sb_{0.5}$ at the EF (E > -5 eV) reflects that there is a notable orbital hybridization between the Bi/Sb-p orbit and the Mn-d orbit, with the electron contribution from the Mn-d orbit being essential but the energy value near -10 eV almost entirely arising from the Bi/Sb-s orbit [Figure 12G]. This observation and the dual line splitting effect of doping, which varies along distinct k-pathways, point to a significant connection between the Mn-d orbitals, ALHA k-paths, and Bi/Sb-p orbitals. The aforementioned authors concluded that in the situation of substitution doping, Sb dopant can be employed as a candidate for the stable phase. Only a tiny quantity of Sb can be doped to the gap position in gap-doped MnBi due to the possibility of increased hybridization between Bi/Sb-p orbital and Mn-d orbital.

In accordance with the studies mentioned above and accounts, quite a few solutions have been implemented to lower the volume expansion of Sb-based anode materials and strengthen their potential for potassium storage: (1) To minimize volume changes and shorten the ion diffusion distance, alter the morphology and structure at the nanoscale; (2) To stop the accumulation of Sb nanoparticles, contain volume variations throughout the cycle, improve electrical conductivity, and utilize carbon materials for buffer layers or conductive structures; (3) The addition of heteroatom doping increases the number of active sites on the surface of carbon-based materials and promotes electrical activity. As a consequence, choosing the proper electrolyte component in accordance with the unique properties of the materials will also aid in increasing the ability of Sb-based anode materials to store potassium. And the practical research on the future large-scale production of Sb-based anode KIBs is intimately tied to the selection and design of appropriate electrolyte components.

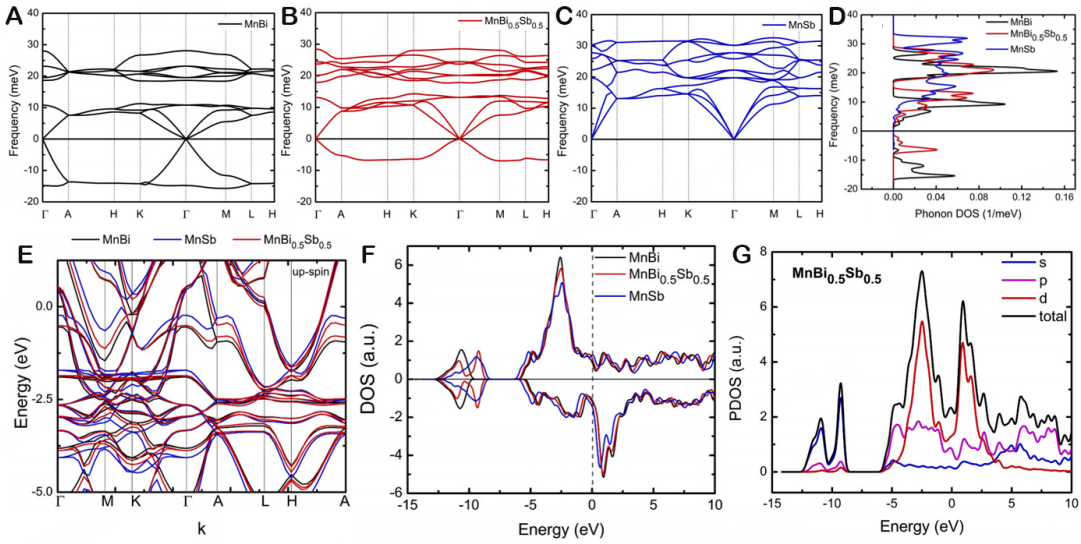

Figure 12. (A-C) Phonon dispersion, (D) phonon density of state, (E) up-spin state band structure, (F) density of states of MnBi, $MnBi_{0.5}Sb_{0.5}$, and MnSb, and (G) Partial density of state of $MnBi_{0.5}Sb_{0.5}$. Copyright2021, Solid State Communications[127].

Sn and its derivative anode for KIBs

Alternative metallic elements that can be alloyed with K have also been investigated as potential KIB anode materials, except that metal Sb. They appear to be a potential option to meet the requirements of the upcoming large-scale energy storage devices due to their low cost and high natural abundance. As a desirable anode material for energy storage devices, tin-based materials offer an extremely specific capacity, a substantial relative concentration, and are environmentally friendly as well[100,128]. In addition, the theoretical capacity of Sn for the LIB and NIB anodes can be up to 990 mAh/g and 847 mAh/g, respectively[129,130]. It is thought that this phenomenon is caused by the contribution of high-density property to the volume energy density of the battery. Sn is, therefore, essential to the investigation of metal-based anode materials for KIBs. Pure Sn also experiences enormous volume changes throughout battery cycling, which may result in electrode material separation and poor battery capacity[131]. Basically, metallic Sn reacts with K through alloying reaction ($Sn + K^+ + e^- \leftrightarrow KSn$) with a theoretical specific capacity of 225 mAh/g. The first study on the electrochemical behavior of a Sn-based anode in a potassium battery was given by Sultana *et al.*[132]. The material has a promising capacity of roughly 150 mAh/g and is active at low potential in comparison to K/K^+. According to experimental data, Sn can be reversibly alloyed or dealloyed with potassium. Combining a metal foil anode (Sn, Sb, K, or Na) and an EG cathode (EC+DMC+EMC), Ji *et al.* developed a unique K double-ion battery[133]. Its special storage mechanism, which offers exceptional capacity retention (93%), is formed up of the PF_6 anion insertion/removal procedure on the graphite cathode and the K^+ alloying/dealloying event on the anode. Yet, the amount of Sn grows significantly after (de-)lithification or (de-)solidification (260% for $Li_{22}Sn_5$ and 420% for $Na_{15}Sn_4$)[134,135]. The volume change of Sn in KIBs is more severe than that of LIBs and SIBs owing to increased K^+[136].

Ramireddy *et al.* conducted a thorough investigation of the K^+ alloying reaction mechanism of Sn thin film electrodes following a range of *in-situ* characterization techniques[137]. After an electrode was fully potassiated, the KSn alloy phase was discovered. Till the initial cycle of potassization/depotassization, a reversible capacity of up to 245 mAh/g was noted. It is interesting that just the second potassium reaction stage revealed the creation of SEI membranes. Besides that, *in-situ* studies of stress variations in Sn film electrodes during potassium/potassium removal cycles prove that mechanical instability happens both during surface reactions and the phase shift caused by potassium alloying and dealloying. Also, research on

the cyclic stability of electrode materials at various operating voltage ranges has found that the ideal value is between 0.01 V and 1.2 V. At the same time, Wang *et al.* reported a study of the K ions storage mechanism of Sn nanoparticles in KIBs using *in situ* TEM and XRD testing[93]. Sn anodes have a 197 mAh/g capacity; however, they are accompanied by serious capacity decay. The results from TEM and XRD analysis reveal that the final alloy in the production of potassium is KSn, which was in accordance with the work of Ramireddy *et al.*[137]. According to *in-situ* TEM, a two-step potassium mechanism with volume changes of 101% and 180% occurred when K_4Sn_9 and KSn alloys were formed, and the development of reversible nanopores during the cycle of Sn nanoparticles precluded the complete recovery of Sn particles. The intense crushing of Sn particles is responsible for the capacity decline that occurs quickly after several cycles. As an example, the metals Sn and K can be alloyed at room temperature to produce a variety of intermetallic compounds, including K_2Sn, KSn, K_2Sn_3, K_2Sn_5, KSn_2, and K_4Sn_{23}[138]. Other charge storage mechanisms have also been proposed in recent years. Despite the fact that these studies highlight some benefits, the Sn element is prone to large volume expansion during the potassium process, which will inevitably result in material crushing and stripping and lower cycling performance and make it more challenging for KIBs to achieve high energy density. Consequently, the Sn-based material modification technique for LIBs and SIBs can also be employed for the K ion system, even though research into Sn-based materials for KIBs has only started. Other approaches to optimizing the capacity of alloy anodes for maintaining potassium, including carbon-based nano-engineering, heteroatom doping, profitable adhesives, and electrolytes, have also made considerable strides.

To further safeguard the active components, graphene can be distributed in CNFs and used as a soft buffer substrate. Additionally, it can improve the conductivity and magnification of materials. Therefore, one of the methods to address this issue is to limit Sn-based alloys to a carbon matrix and introduce the method of dealloying to create porous metal particles by alloy corrosion[112,139]. Ge *et al.* expressed Sn nanoparticles in the non-graphitized carbon in the Sn-C composite made by mechanical ball milling for the first time, and they have a capacity of 150 mA h/g as the anode of NIBs[140]. The KIB anode is, therefore, predicted to have a reversible capacity of between 150 mA h/g and 190 mA h/g when the carbon content of an electrode is taken into account. Qin *et al.* developed a 3D porous graphene network using 3D self-assembly as a template, encasing Sn nanoparticles inside a graphene shell (Sn@G-PGNWs), as shown in Figure 13A[141]. In addition to successfully preventing Sn from coming into direct contact with the electrolyte, the highly elastic graphene shell created by Chemical Vapor Deposition (CVD) also helps to preserve the structure and interface stability of Sn nanoparticles. Sn@G is a tightly fixed 3D porous graphene network with great mechanical flexibility, huge surface area, and good conductivity. It is possible to considerably increase the conductivity and structural integrity of the entire electrode. As such, porous carbon materials that serve as the buffer layer may assist in maintaining the integral design of composite electrodes. Huang *et al.* built a 3D carbon/Sn porous polymer (3D-HPCS) anode utilizing a NaCl template[142]. The performance of potassium storage is improved by the enormous surface area of Sn nanoparticles and composites uniformly placed in 3D porous carbon. This can somewhat reduce the volume expansion during the (de-)potassium process. The initial Coulombic efficiency (ICE) exceeding 96% and the reversible capacity of up to 276.4 mAh/g imply that non-uniform structures are also vital for the efficacy of potassium storage. Via the sol-gel technique, Yang *et al.* created N-doped porous carbon materials (Sn/NPC)[143]. Given their distinctive shape, strong conductivity, and substantial surface area, Sn/NPC electrodes have an amazing ability to store potassium. As illustrated in Figure 13B, Li *et al.* described the hierarchically porous carbon-supported Sn_4P_3@C composite as an anode material for KIBs first[144]. According to a number of characterization techniques and electrochemical performance research, Sn_4P_3@C undergoes a three-phase transformation into Sn, KSn, and K_4Sn_{23} during the whole discharge process. And then, due to the fact that graphene sheets may successfully prevent Sn_4P_3 nanoparticle aggregation and enhance electronic conductivity, Du *et al.* created Sn_4P_3/multilayer graphene sheets (Sn_4P_3/MGS) composites by impregnating Sn_4P_3 nanoparticles into

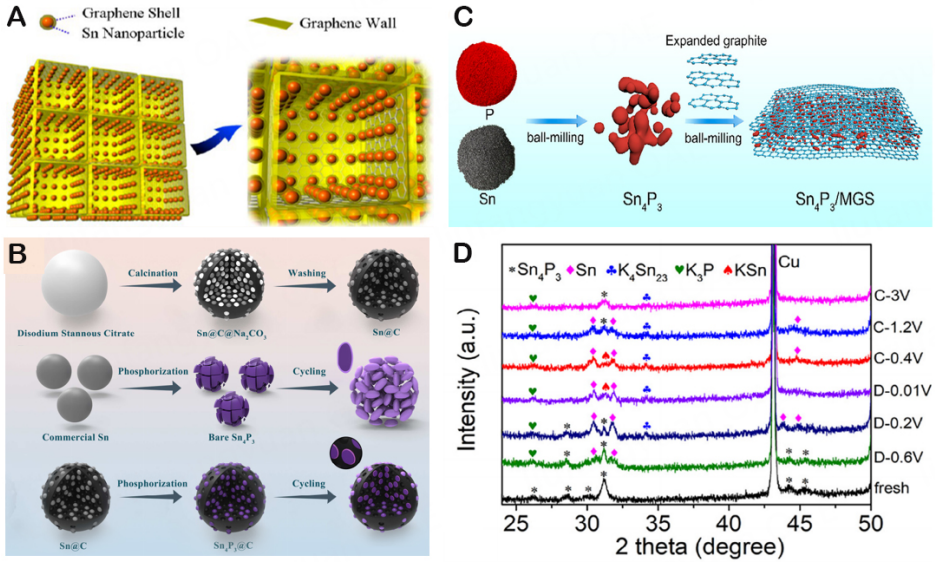

Figure 13. (A) Schematic illustration of 3D Sn@G-PGNWs. Copyright 2014, ACS Nano[141]. (B) Schematic illustration of the synthesis of Sn_4P_3 and Sn4P3@C. Copyright 2019, Energy Storage Materials[144]. (C) Schematic illustration of the synthesis of Sn4P3/MGS-80. (D) The *ex-situ* XRD patterns of the Sn_4P_3/MGS electrode at different discharge/charge states. Copyright 2021, Journal of Energy Chemistry[145].

graphene sheets [Figure 13C][145]. Additionally, nanoparticle impregnation increases the surface area of contact of the electrolyte, reducing the diffusion distance of K^+. With regard to this, the improved Sn_4P_3/MGS has a high reversible capacity and magnification performance of 378.2 mAh/g at 0.1 A/g. During the discharged process [Figure 13D], the peak of Sn_4P_3 drops significantly, and the Sn phase, K_3P phase, K_4Sn_{23} phase, and KSn phase appear once. Later in the charging process, there is a gradual regeneration of the corresponding peak Sn_4P_3. The peak is still related to some discharge products, suggesting that the conversion and alloy reaction of potassium/potassium in Sn_4P_3/MGS materials are partially reversible. Then, applying electrospinning technology, Li *et al.* accurately constructed N-doped porous Sn nanosphere composites (Sn/N-CNFs)[146]. In comparison to other Sn-based materials, Sn/N-CNFs have superior cycling stability as KIB anodes (198.0 mAh/g at 1 A/g after 3,000 cycles), with a corresponding capacity retention rate of 88.4%. The mechanism underlying the electrochemical performance of Sn/N-CNFs in KIBs is revealed as follows: To begin with, the interaction between extremely small nanoparticles within Sn nanospheres simplifies the ion migration path and yields a buffer space for volume expansion and contraction. The presence of a carbon framework expands electronic conductivity by preventing the agglomeration of internal Sn nanoparticles. The notably linked CNFs also support a significant improvement in the reversible and rate capacity of Sn/N-CNFS as KIB anodes by offering a viable transmission channel for electrons while conserving structural integrity.

For designing ideal high-capacity Sn-based KIBs, effective procedures, such as structural modification, nanomaterialization, combining conductive materials, and interface management, have a major practical value. In spite of several studies on tin-based anodes in recent years, research into the development of tin-based anodes in KIBs, which include intricate reaction mechanisms, potassium storage mechanisms, suitable electrode materials, electrolytes, *etc.*, is still in its early phases. In 2020, Yamamoto *et al.* manufactured KIBs utilizing liquid electrolytes containing bis (fluorosulfonyl) amide ions to match submicron-sized Sn particles, increasing the capacity retention rate of the Sn negative electrode over 170 mAh/g[147]. This paved the way for a thorough investigation into how various electrolytes can improve the capacity of KIBs for potassium storage.

P and its derivative anode for KIBs

P compounds, such as white, red, and BP, have also been investigated as prospective anode materials for KIBs, with a theoretical capacity of up to 843 mAh/g, as evidenced by LIBs and SIBs[148,149]. Among them, white P cannot be utilized as an electrode material for scientific study since it is poisonous, volatile, unstable, and combustible in the air. Non-toxic and comparatively stable, amorphous RP can store ions (Li^+, Na^+) in an amorphous form. However, its poor conductivity and significant volume growth restrict its practicality[150]. Lastly, during the high-temperature and high-pressure transition of RP into white P, an occurrence of BP was observed. Its exceptional 2D layered structure and superior conductivity render it perfect for the creation of high-performance KIBs. However, the harsh synthetic conditions for obtaining BP are difficult problems that must be solved[151]. Likewise to SIB and LIB, the alloying reaction of manufacturing K_xP is thought to be the basic mechanism of RP in KIBs based on the existing three-electron mechanism[152]. Although K_3P theoretically holds a very high capacity of 2,596 mAh/g, no empirical findings have proven this claim[153,154]. On the other hand, the potassium method caused the production of KP and K_4P_3 alloys with corresponding capacities of 865 and 1,154 mAh/g[155]. Hence, the latest objective of the studies of scientists is to figure out the development direction and response mechanism of the P anode in KIBs[156,157]. With the support of a template method and a unique alloying mechanism (4K + 3P K_4P_3), Wu *et al.* created RP nanoparticles by encapsulating them in N-doped porous hollow CNFs [Figure 14A][92]. This results in RP possessing an excellent theoretical capacity of 1,154 mAh/g. Also, they noticed that the synthesis of potassium phosphate compounds and the following alloying processes caused the generation of K_4P_3, as shown in Figure 14B, which was supported by *in-situ* Raman and non-*in situ* XRD data. Lastly, Xiong *et al.* confirmed the creation of KP through research of potassium storage mechanism on RP@carbon nanosheet composite[158]. The DFT evaluation of the K-P phase diagram implies that KP may possess stable thermodynamic properties with the lowest formation energy. Moreover, within high-performance KIB anode materials, the single-electron reaction (P + K^+ + e KP) featuring a theoretical capacity of 843 mAh/g is thought to be the greatest and most realistic potassium reaction. In addition, using DFT calculations, Kim *et al.* computed the energetics of K and P alloying[99]. The most reliable alloying product configurations, which equate to 865 mAh/g and 1,154 mAh/g in theoretical capacity, are KP and K_4P_3. Since alloying voltage of K_4P_3 is lower than that of KP, the matching KIB system will have a larger energy density. Meanwhile, a mechanism to ascribe potassium products to partially crystalline or amorphous $K_{3-x}P$ was put out by Zhang *et al.*[159]. As observed in Figure 14C, the binary K-P system exhibits the stages KP, K_4P_3, K_3P_{11}, and K_3P when the cyclic P/C electrode is discharged to 0.5 V or 0.01 V. Then, a recent DFT calculation by Yang *et al.* also postulated the alloying reaction mechanism of BP in KIBs[160]. Figure 14D illustrates how the formation energies of many potential K-P alloy phases, including K_3P_{11}, K_3P_7, K_2P_3, KP, K_4P_3, and K_3P, were calculated during the potassization process. Since the K_3P_7 point separates from the energy curve for fairly low formation energy, this phase really is not generated during the potassification process. Additionally, due to the extremely negative potential of KIBs, K_3P cannot exist, which is in contrast to the three-electron alloying mechanisms in LIBs and SIBs. This will restrict the capacity of KIB BP to take in potassium. Graphite will be considered in future calculations for the KIB since the graphene layer in the P/G heterostructure can serve as a buffer to help adapt to the volume expansion of BP during the sodium reaction. By encasing BP particles within sizable graphite particles, Yang *et al.* successfully created a BP/carbon composite anode for KIBs[160]. Nevertheless, a number of electrochemical characterization methods reveal that even in ideal circumstances, only 500 mAh/g of reversible capacity is observable. The capacity loss rate reaches 40% after 50 cycles. BP as the KIB anode continues to be difficult to employ at this time. The exorbitant cost of BP may also make it difficult to use. One of the major future prospects is the development of low-cost synthetic BP techniques.

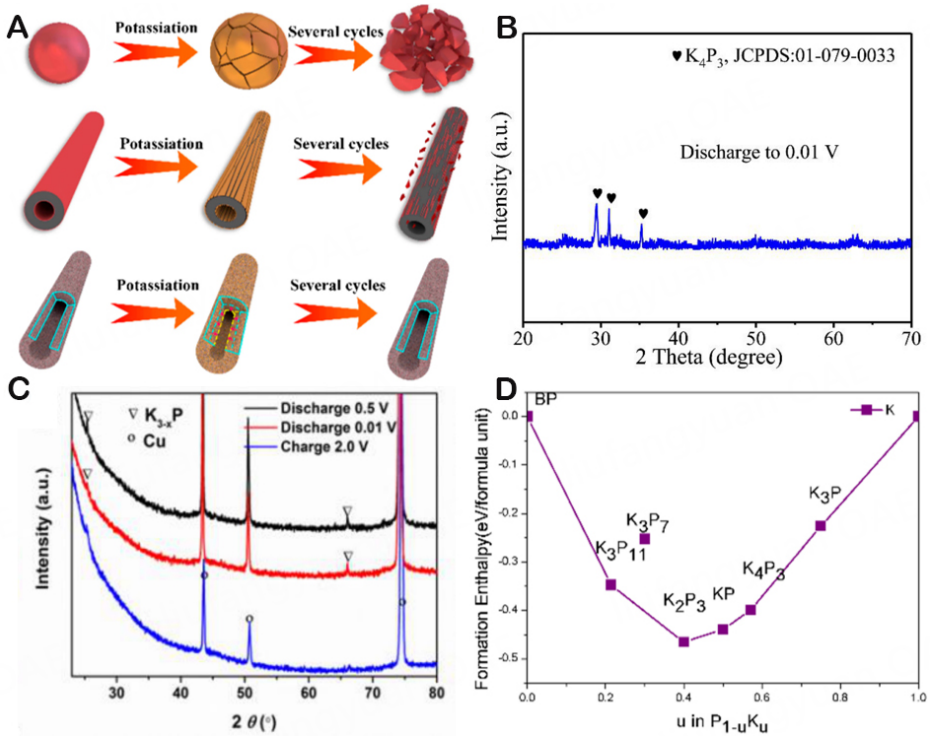

Figure 14. (A) Schematic illustration of the (de-)Potassiation process of red P particles, hollow carbon fibers coated with red P, and nanostructured red P confined in the N-PHCNF matrix in KIBs. (B) *In-situ* XRD patterns of the red P/N-HCNFs-5 composite when discharged to 0.01 V. Copyright 2019, Nano Letters[92]. (C) P/C electrodes in KIBs at different potentials. Copyright 2017, Journal of the American Chemical Society[159]. (D) Formation energies of possible phase during potassiation for BP. Copyright 2019, Electronic Materials Letters[160].

Despite having a large theoretical specific capacity (2,596 mAh/g), pure P exhibited a very poor specific charge capacity and CE, which severely restricts its broad use in the filed of KIBs. In particular, due to significant volume growth during the charge-discharge operation, the pure RP and BP anodes deliver very low reversible capacity. According to weak electrochemical involvement and strong polarization of RP, active materials for ion storage have limited electrical conductivity[154]. Low redox kinetics can then impair cycle performance, especially when there is a high current density. Higher battery polarization can cause the formation of uneven SEI films and the excessive decomposition of electrolytes, resulting in low ICE and significant capacity degradation as electrode materials[149]. In brief, the development of P anodes for KIBs has advanced significantly, but there are still numerous obstacles to overcome, including poor electronic conductivity[92], significant volume expansion[161], and an unstable SEI. These challenges will also cause capacity decay and poor coulomb efficiency[162]. Researchers are now looking into the optimization of modification techniques for high-performance anode materials in an attempt to eliminate the barrier witnessed by the aforementioned KIB utilizing P anode materials. Recent studies have mainly focused on the combination of carbon-based materials to establish heterostructure, heteroatom doption, and electrolyte composition optimization. In 2019, Chang *et al.* used a straightforward one-pot wet-ball milling (WBM) technique to effectively create a KIB anode with excellent performance RP[163]. The RP/C electrode has a high reversible specific capacity (750 mAh/g) and excellent rate capacity, which can be attributed to the assistance of the conductive network made of multi-walled CNTs and the equally dispersed nanoscale RP particles, making RP an appealing anode material for K ion storage. In particular, it is hypothesized that the absence of a P-C bond facilitates the efficient reaction of the K^+ with the RP, which is based on the examination of electrochemical measurement. However, Wu *et al.* manufactured phosphorous/carbon

composites using a straightforward mechanical ball milling procedure and investigated them as KIB anode materials[157]. The findings indicate that the P/C electrode has a high capacity of 323.5 mAh/g, medium cycle stability, and rate performance. This is primarily attributable to the high theoretical specific capacity of P and the homogeneous distribution of amorphous BP in the carbon matrix by ball milling, which forms a steady P-carbon bond and effectively inhibits the volume expansion in the process of potassium and potassium removal [Figure 15A]. Ball milling is useful for promoting intimate contact between primary particles, conductive carbon matrix and P, and the viability of P/C composites with rich P-C or P-O-C chemical bonds, but it is still unable to further reduce the particle size of P to the nanoscale level. Since there was insufficient electrical contact between the collector and the active material and the limited carbon covering, which was unable to react to the significant volume shift of the P anode, performance eventually suffered. As a result, it needs to be used in conjunction with other synthesis techniques in order to significantly raise the electrochemical performance of P anodes. And then, the growing trend of the P anode is still limited by its intrinsic insulating properties and significant volume fluctuations. To overcome this situation, Liu *et al.* combined RP with mesoporous carbon (TBMC) and CNTs to create a special P@TBMC Composite material[164]. Multi-walled CNTs can hasten electron transmission because they contain a lot of sp^2 carbon, while the mesoporous carbon layer can be used to load the right amount of P and act as a buffer layer to reduce the extreme volume expansion. Thus the P@TBMC composite performs admirably as a KIB anode in terms of reversible specific capacity, cycle performance, and rate capacity. The creation of high-performance electrode materials is facilitated by the design that restricts the active component to hybrid carbon nanostructures combined with highly conductive sp^2 carbon and porous carbon.

The introduction of carbon materials into P-based anode materials may significantly increase rate performance and structural stability owing to their larger surface area and powerful conductivity. For instance, Fang *et al.* synthesized an air-stabilized RP anode that improves electronic conductivity by isolating the active substance from direct contact with the electrolyte [Figure 15B][165]. The composite as a potassium electric anode presents reversible capacity and long cycle life, which is mainly attributed to the RP-activated carbon (P@AC) composite surface coated conductive polypyrrole (PPy) layer can prevent air oxidation, protect the RP material, and improve the structural stability of active materials. Additionally, Wu *et al.* added RP to N-doped porous hollow CNFs (RP@N-PHCNFs) to keep P particles from being crushed and aggregated[92]. Since the establishment of P-C chemical bonds in the carbon matrix and N doping, the composite fibers exhibit good structural stability during the potassium process, according to electrochemical measurements. A theoretical P-adsorption ability of the N-doped carbon matrix is estimated using DFT calculation to further highlight how N doping on the N-PHCNF matrix improves the potassium storage efficiency of the RP@N-PHCNF anode. Figure 15C displays the equivalent undoped and N-doped carbon defect models. The calculations indicate that the bridge site-the midpoint of a C-C bond for undoped graphene and the midpoint of a C-C bond next to a N atom for N-doped graphene - is the most stable location for P atom adsorption sites. Additionally, the predicted adsorption energies for a single P atom in undoped and N-doped graphene are 1.52 eV and 2.22 eV, respectively. These findings show that the N-doped carbon matrix has a substantially higher attraction for adsorption than that of the undoped one, which results in a strong and close bond between RP and the N-PHCNF carbon matrix. The strong ability of RP@N-PHCNF anodes to store potassium is a result of their chemical adsorption function. Furthermore, through the one-step synthesis of self-template and recrystallization-self-assembly technique, Bai *et al.* first investigated the potassium storage performance of the core-shell (several nanometers) CoP anode embedded in the N, P co-doped porous carbon sheet matrix (CoP ⊂ NPPCS)[166]. A single precursor can be created by utilizing the anomalous coordination properties of melamine and metal ions as well as the hydrogen bonding synergy between melamine and phytic acid to create a 2D network. In addition, Wang *et al.* prepared RP@rGO composite material by vaporization–condensation method[167]. RP particles can be anchored on the rGO plate to increase both its structural stability and conductivity during the

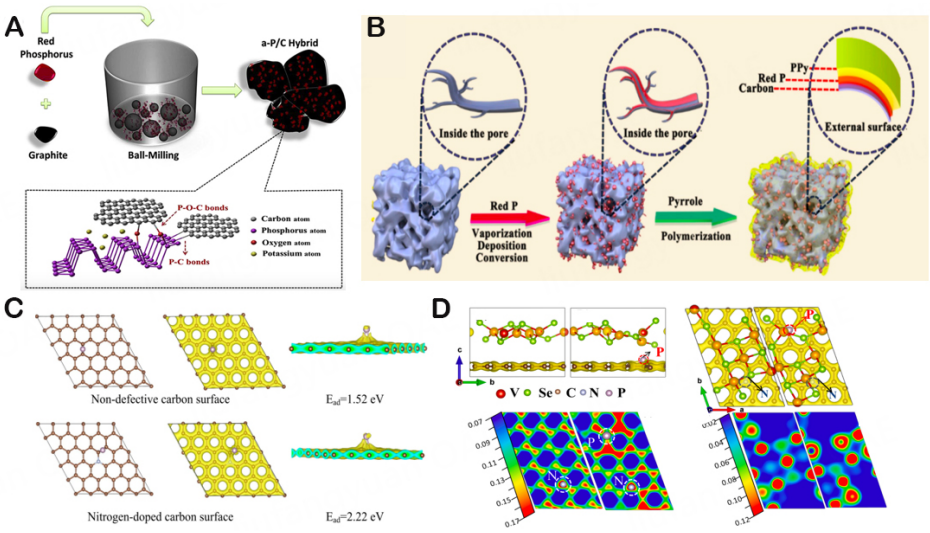

Figure 15. (A) Schematic diagram of the synthesis of the P/C composite. Copyright 2018, Journal of Power Sources[157]. (B) Schematic illustration of the fabrication process of red P@AC and red P@AC@PPy composite. Copyright 2020, Nano energy[165]. (C) DFT computations of P atoms adsorbed on nondefective or nitrogen-doped carbon surface and corresponding adsorption energy (E_{ad}). The brown, blue, and red balls represent C, N, and P atoms, respectively. Copyright 2019, Nano Letters[92]. (D) The corresponding three-dimensional charge density and two-dimensional charge density maps in V_3Se_4/CNF system and V_3Se_4/NPCNF system, respectively. The three-dimensional charge density par value is set at 0.14 e/bohr^3. Saturation values are marked on the two-dimensional charge density scale, and high values correspond to electron abundance. Copyright 2021, Chemical Engineering Journal[168].

alloying and dealloying process. The superior conductivity and solid structure of the composite matrix, which can significantly increase the electronic conductivity of the electrode, are primarily responsible for good electrochemical performance. Additionally, through an alloying mechanism, P particles can contribute highly. Moreover, Xu *et al.* successfully embedded V_3Se_4 nanoparticles into N/P co-doped CNFs by biomass algae[168]. DFT calculations were used to further explore the effect of N/P co-doping on electrochemical properties. As shown in Figure 15D, highly electronegative P atoms break the electric neutrality of the material, and charge tends to accumulate at the P doping site, which makes V_3Se_4/NPCNF composite materials possess stronger ion adsorption capacity and cycling stability. A selection of observations proves that N/P co-doping may accelerate the ion reaction kinetics and regulate the spacing of electrons in KIBs, boosting its capacity for potassium storage.

In addition, the use of P in electronic equipment is also constrained by various flaws. High carrier mobility and magnetism are vital for spintronic devices, which motivates researchers to keep investigating the electrical structure and magnetic properties of materials. Doping is a dependable and effective way to change the electrical structure of 2D materials and introduce magnetism. Nowadays, a novel 2D material known as a phosphor that possesses higher ranges of magnetic and electron mobility at ambient temperature has been successfully extracted from black phosphor block by mechanical stripping[169]. Currently, Te-doped phosphors have been made by Zhang *et al.* using chemical vapor transfer, while Viti *et al.* have obtained Se-doped black phosphors for 2D photodetectors[170,171]. In order to examine how Ce and Ti substitution doping affect the magnetic moment change in non-magnetic phosphors, Hussain *et al.* applied by the DFT theory based on the generalized gradient approximation approach to obtain the DOS of an impurity-doped phosphorene of different electronic configurations (P, Ti, and Ce) [Figure 16A][172]. It is evident that the systems with Ti-up, Ti-dn, and Ce-Ti pair doping exhibit weak magnetic activity. Ce-up and Ce-dn really do not behave magnetically or metallically halfway. Nevertheless, Ce-Ce couple-doped systems and Ti-Ti couple-doped systems exhibit magnetic and semi-metallic behavior since the spin

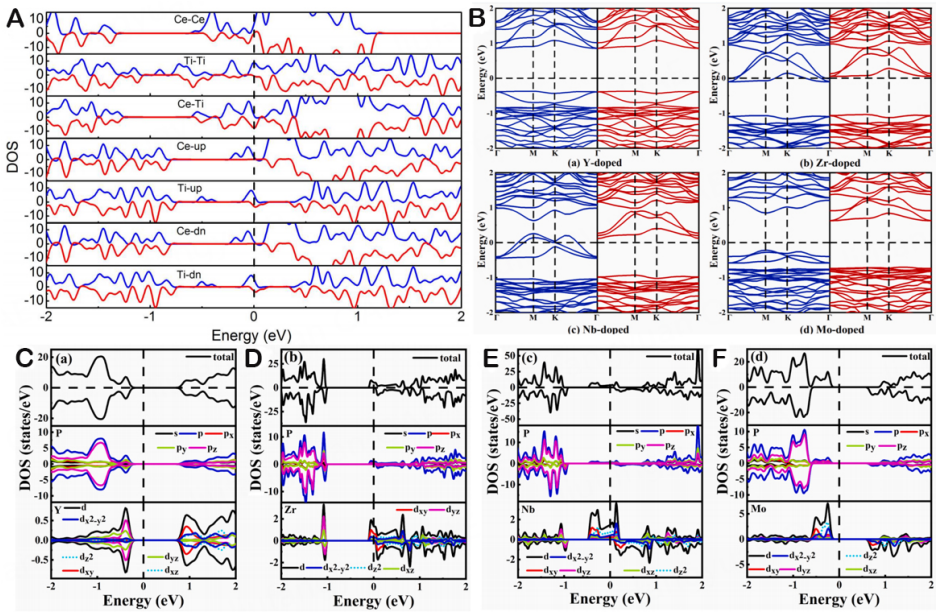

Figure 16. (A)The spin-polarized DOS of Ce-Ce, Ti-Ti, Ce-Ti, Ce-up, Ti-up, Ce- dn, and Ti-dn, respectively. Copyright 2019, Nano Structures[172]. (B) Band structures of Y-, Zr-, Nb-, and Mo-doped blue phosphorene by substitutional doping method. The blue lines (red lines) represent the spin-up (spin-down) channels. The Fermi level (EF) represented by a dotted line is set at E = 0 eV. The TDOS and PDOS of (C) Y-, (D) Zr-, (E) Nb-, and (F) Mo-doped blue phosphorene by substitutional doping method. The EF is set at zero energy and indicated by the vertical black dashed line. Copyright 2021, Thin Solid Films[173].

polarization of majority and minority spin channels crosses the EF. The valence and conduction bands of atomic orbitals react with magnetic dopants to generate magnetic and semi-metallic characteristics. These findings show that each impurity doping has unique bonding properties. What is more, Duan *et al.* successfully reported the geometrical, electronic, magnetic, and optical properties of blue phosphorene doped with yttrium (Y), zirconium (Zr), niobium (Nb), and molybdenum (Mo) can be improved via DFT calculations[173]. The computed binding energy of Y-, Zr-, Nb-, and Mo-doped blue phosphors is positive (8.1 eV, 9.04 eV, 11.34 eV, and 10.28 eV, respectively), indicating that the doping procedure is favorable energetically. Consequently, the binding energy is higher than that of atomic doping on blue phosphor, which is in the 8.10-11.34eV range. By definition, a more stable doping structure corresponds to a greater absolute value. Figure 16B displays the spin-polarized structure that was created through substitution doping. Since the spin-up and spin-down curves for the Y-doped system are consistent, induced spin polarization is not present. The indirect band gap of the Y-doped system is 1.23 eV, and it still exhibits non-magnetic semiconductor properties. Moreover, the system doped with Zr and Nb exhibits semiconductor properties in the spin-down channel while passing through the EF in the spin-up channel. The data demonstrate that Zr and Nb-doped systems exhibit semi-metallic properties. Additionally, they exhibit 100% spin polarization close to the EF, indicating that they are excellent spintronics candidates. And then, the TDOS and PDOS of Y-, Zr-, Nb- and Mo-doped systems are plotted in Figure 16C-F. The spin-up and spin-down channels in the Y-doped system are entirely symmetrical, which suggests that the system is not magnetic, according to the TDOS. The spin-up and spin-down channels, however, are asymmetric for single-layer phosphors doped with Zr, Nb, and Mo, indicating that they are magnetic. The spin-up channel for Zr-doped and Nb-doped systems crosses the EF, while the EF is found in the band gap of the spin-down channel, indicating that these systems have semi-metallic properties. It is critical to remember that the 4d orbitals of the Zr and Nb atoms are the primary source of spin polarization, which means that the unpaired 4d electrons of these atoms are the primary source of magnetism. The spin-up and spin-down channels are asymmetric in the Mo-doped system, and a diluted magnetic semiconductor can be seen in the open band

gap. They discover that the Mod_{xy}, Mod_{x2-y2}, and Mod_{z} orbits around the EF also significantly contribute to the spin polarization from the PDOS curve of the Mo-doped system. The aforementioned findings demonstrate that blue phosphors doped with Y, Zr, Nb, and Mo can be utilized as thin film materials in the fields of nano-spintronics and optoelectronics and also offer a fresh concept for the future magnetic research of P-based materials.

CONCLUSION

This article comprehensively discusses the mechanism and structure-activity relationship of carbon-based and alloy-based anodes with high performance, interface stability, and energy storage mechanisms, and the specific performance is shown in Table 1. Carbon materials are superior to many other materials because of their high conductivity, low cost, and non-toxic properties. In addition, heteroatom doping and nano-engineering can significantly improve the potassium storage performance of carbon-based materials. For example, N doping can improve the adsorption energy and electronic conductivity of K ions, which helps to quickly embed or detach ions or electrons and maintain structural integrity. In addition, carbon-based materials with nanostructures have strong structural stability, which can reduce the diffusion path of ions and ensure excellent electrochemical capability. Alloy-based materials are attributed to their good working voltage and strong theoretical specific capacity, making them one of the most promising candidate materials in KIBs. At present, the problems of scale production of KIBs mainly focus on excessive volume expansion, short cycle life, and low initial coulomb efficiency during charging and discharging. Therefore, future research may gradually shift from structural design to alleviating volume expansion and improving electronic conductivity, further promoting interface stability and capacity reversibility. Several possible research options are listed as follows:

(1) Alloying and heterostructures may become the primary targets of structural design and morphological optimization due to significant studies on basic materials. Unique qualities that set it apart from ordinary additions may come from material design. However, not all unique structural designs are advantageous without any drawbacks, such as the nanoscale method that gives alloy-based materials a lot of specific surface area while also consuming a lot of electrolytes. Therefore, the balance between particle size and specific surface area should be taken into account while designing structures.

(2) Equally important is the choice of anode materials that serve as K^+ carriers in the electrochemical process. Apart from the carbon-based and alloy-based anode materials discussed above, they also include other types of anodes, such as intercalation anodes, conversion anodes, organic anode materials, and so on. Potassium metal was originally the chosen anode material for high-performance KIBs due to its large theoretical capacity. However, potassium metal undergoes excessive chemical reactions with the electrolyte components, forming an unstable SEI layer and increasing electrode polarization during the entire charging and discharging process attributed to its high chemical reactivity, leading to a noticeably lower capacity. Additionally, owing to its volume expansion, high air oxidizability, and associated safety considerations, it has gradually been removed from the list of possible anode materials for KIBs. Moreover, it has a reduced energy density as an electrode material because of its low specificity and high operating voltage. Nevertheless, due to their high theoretical specific capacity and distinctive pseudo capacitance phenomenon, transition metal oxides, transition metal sulfides, transition metal selenide, and other conversion anode materials generated great concern among researchers. But innate flaws, such as poor conductivity and significant volume expansion, have a negative impact on the performance of electrode materials. To enhance its electrochemical performance, it is typically coupled with carbon-based materials or constructed with suitable nanostructures. Additionally, organic molecules can provide more buffer space between one another, which enhances the ability of electrode materials to store potassium. However, its

Table 1. Recent progress on carbon-based and alloy-based anode materials in KIBs

Materials	Charge capacity (mA/g)	Rate capacity	Capacity retention	Refs.
K_2TP	229 (200 mA/g)	-	94.6%	[26]
NOPC@G	445	112 (40 C)	-	[28]
MG	115 (4 A/g)	-	75% (20,000 cycles)	[31]
PODG	474 (50 mA/g)	-	160 mAh/g (2,000 mA/g)	[33]
HC/CB	200 (0.1 C)	-	57% (685 cycles)	[36]
HCS	262	-	83% (100 cycles)	[38]
HC-HCl	253 (40 mA/g)	164 (4 A/g)	92% (150 cycles)	[39]
HHC	195.3 (0.1 A/g)	-	67.43% (150 cycles)	[40]
LPG	150 (100 mA/g)	70 (200 mA/g)	225 mAh/g (400 cycles)	[45]
NCS	154 (72 C)	-	180 mAh/g (4,000 mA/g)	[49]
CoSe/C	597.2 (0.2 A/g)	-	361.9 mAh/g (16 A/g)	[50]
HN-CFA	282 (0.1 A/g)	175 (5 A/g)	249 mAh/g (7,000 cycles)	[51]
A-KBT-7	496.1 (50 mA/g)	-	102.1 mAh/g (2,300 cycles)	[52]
SP-HC	284 (0.1 C)	167(1C)	71% (300 cycles)	[53]
CNF	210 (1 A/g)	-	100 mAh/g (7.7 A/g)	[59]
CNC	175 (35 C)	-	79% (35 C)	[60]
OCFGs	370.2 (0.2 A/g)	137 (4 A/g)	-	[61]
MHCNFs	329.1 (100 mA/g)	268.5 (5,000 mA/g)	252.6 mAh/g (2,500 cycles)	[63]
PCMs	226.6 (50 mA/g)	158.1 (1,000 mA/g)	108.4 mAh/g (2,000 cycles)	[64]
HG-CNFs	200	226 (35 C)	fade 0.008% (400 cycles)	[67]
NCNFs	248 (25 mA/g)	101 (20 A/g)	146 mAh/g (4,000 cycles)	[71]
HPNCFs	197 (50 mA/g)	57 (250 mA/g)	197 mAh/g (90 cycles)	[72]
NPCF	327 (100 mA/g)	144 (10 A/g)	258.9 mAh/g (2,000 cycles)	[73]
N-SPC	288 (0.2 A/g)	116 (20 A/g)	296 mAh/g (2,000 cycles)	[75]
PN-PCM	396 (0.1 A/g)	168 (5 A/g)	218 mAh/g (3,000 cycles)	[76]
PIBN-G	271 (0.1 C)	-	86% (300 cycles)	[88]
red P@N-PHCNFs	465 (2 A/g)	342 (5 A/g)	465 mAh/g (2 A/g, 800 cycles)	[92]
$Bi_{0.5}Sb_{0.5}$@P	339.1 (1 A/g)	258.5 (6.5 A/g)	295.4 mAh/g (500 mA/g, 550 cycles)	[94]
8-Sn@C	493.6 (200 mA/g)	349 (4,000 mA/g)	415 mAh/g (1,000 mA/g, 500 cycles)	[100]
S-BC	339.3 (50 mA/g)	124.2 (1 A/g)	203.8 mAh/g (200 mA/g, 300 cycles)	[102]
CoS@CNF-CNT/EG	411	184 (2 A/g)	84.9% (100 cycles)	[107]
Sb@rGO	381 (100 mA/g)	-	210 mAh/g (500 mA/g, 200 cycles)	[109]
$Sb_4O_5Cl_2$	530 (50 mA/g)	316 (100 mA/g)	-	[111]
Co_3O_4-Fe_2O_3/C	220 (50 mA/g)	-	93% (180 cycles)	[112]
Sb@G@C	474 (100 mA/g)	-	72.3% (800 cycles)	[113]
Sb@NPMC	384.8 (50 mA/g)	130 (1 A/g)	-	[114]
NP-Sb	560 (50 mA/g)	265 (500 mA/g)	-	[116]
Sb-C-rGO	310 (0.5 A/g)	-	79% (100 cycles)	[117]
Sb@C-3DP	516 (0.05 A/g)	286 (1 A/g)	97% (260 cycles)	[119]
Sb_2Se_3@C	312.8 (100 mA/g)	223.3 (1 A/g)	191.4 mAh/g (500 mA/g, 400 cycles)	[123]
BiSb@C	598.2 (100 mA/g)	152 (2 A/g)	97.5% (500 mA/g, 600 cycles)	[124]
Ti_3C_2-Sb_2S_3	461 (100 mA/g)	102 (2 A/g)	79 % (500 cycles)	[125]
SnO_2-G-C	-	114.81 (1 A/g)	202.06 mAh/g (100 mA/g, 100 cycles)	[139]
Sn_4P_3@C	473.3 (50 mA/g)	183.6 (2A /g)	181.5 mAh/g (500 mA/g, 800 cycles)	[144]
PAC-50	430	-	70% (500 cycles)	[156]
P@CN	655 (100 mA/g)	323.7 (2 A/g)	-	[158]

practical application is restricted by the lower energy density (low material density) and poor electronic conductivity. In order to address this issue, the electrode preparation procedure can include the proper addition of conductive carbon and active materials.

(3) To build an industrial chain for realistic large-scale production, it will be crucial to investigate the performance of carbon- and alloy-based anode materials of full-cell KIBs. The matching of full-cell KIBs necessitates a thorough investigation of the electrochemical reaction processes between the cathode, anode, and various electrolytes in order to obtain high capacity and energy density. The performance of PIB full batteries has received relatively few research reports to date. For instance, Zhao *et al.* utilized Prussian blue potassium (KPB) and ZnSe/$CoSe_2$@N-CNTs /rGO assembled full battery, exhibiting a capacity of 151 mAh/g at 100 mA/g[174]. And Sun *et al.* successfully assembled full-cells of $CoSe_2$/C//PTCDA-450 for KIBs, which possess a good rate performance[175]. Yet, these KIB full batteries have limited capacity and energy density, demonstrating that there is still more work to be done in the research and development of full-cell KIBs.

(4) Safety has always been the focus of attention for KIBs. The primary concern raised here is the propensity for explosive reactions of potassium metal anodes with highly flammable organic electrolytes and potential safety risks, such as short circuits, overheating, and explosions. This can be accomplished by creating potassium batteries that are entirely solid-state, creating potassium metals with complex structures and stable interfaces, or employing liquid alloys based on alkali metals. Additionally, employing flame retardant electrolytes, ionic liquid electrolytes, and all solid electrolytes can reduce the flammability of electrolytes and their combinations, which can enhance safety to some extent.

(5) Within this overview, the potassium storage mechanism of KIBs developed for carbon- and alloy-based anode materials was thoroughly investigated via DFT theory calculations, and positive evidence is given for multiple modification strategies to enhance the potassium storage capacities of the materials. Meanwhile, the worth of material calculation simulation extends beyond this and involves the following: (1) separate the influence parameters in experimental conditions as a single factor to explore their contribution to experimental results and then find internal laws to reasonably explain experimental phenomena; (2) predict the characteristics of novel materials; (3) simulate experimental processes under extreme conditions or super ideal states and; (4) establish a new structural model based on comprehensive experimental conditions, analyze and establish a new theoretical system, *etc.* The primary DFT algorithms contain the molecular dynamics algorithm, the forward (reverse) Monte Carlo method, and the first-principles algorithm. In-depth investigation and exploration are the activities we need to complete next while our comprehension and implementation of DFT theoretical calculations are still in stages of development.

DECLARATIONS

Authors' contributions

Searched a large amount of literature, wrote a complete manuscript, and obtained copyright licenses for all cited images in the manuscript: Chen Y, Sun H
Provide the research direction and funding support: Zhang Z
Helped to guide the review, including language checking and polishing: Li WJ, Chou S, Jiang Y
Image organization and layout: Guo J, Zhao Y, Yang H, Li H

Availability of data and materials

Not applicable.

Financial support and sponsorship
This work was financially supported by the National Natural Science Foundation of China (No. 52271011).

Conflicts of interest
All authors declared that there are no conflicts of interest.

Ethical approval and consent to participate
Not applicable.

Consent for publication
Not applicable.

REFERENCES

1. Yuan F, Zhang W, Zhang D, et al. Recent progress in electrochemical performance of binder-free anodes for potassium-ion batteries. *Nanoscale* 2021;13:5965-84. DOI
2. Wu Y, Zhao H, Wu Z, et al. Rational design of carbon materials as anodes for potassium-ion batteries. *Energy Stor Mater* 2021;34:483-507. DOI
3. Yang M, Kong Q, Feng W, Yao W. N/O double-doped biomass hard carbon material realizes fast and stable potassium ion storage. *Carbon* 2021;176:71-82. DOI
4. Yang M, Kong Q, Feng W, Yao W, Wang Q. Hierarchical porous nitrogen, oxygen, and phosphorus ternary doped hollow biomass carbon spheres for high-speed and long-life potassium storage. *Carbon Energy* 2022;4:45-59. DOI
5. McCulloch WD, Ren X, Yu M, Huang Z, Wu Y. Potassium-ion oxygen battery based on a high capacity antimony anode. *ACS Appl Mater Inter* 2015;7:26158-66. DOI
6. Han Y, Li T, Li Y, et al. Stabilizing antimony nanocrystals within ultrathin carbon nanosheets for high-performance K-ion storage. *Energy Stor Mater* 2019;20:46-54. DOI
7. Ma L, Lv Y, Wu J, et al. Recent advances in anode materials for potassium-ion batteries: a review. *Nano Res* 2021;14:4442-70. DOI
8. An Y, Fei H, Zeng G, et al. Commercial expanded graphite as a low-cost, long-cycling life anode for potassium-ion batteries with conventional carbonate electrolyte. *J Power Sources* 2018;378:66-72. DOI
9. Jian Z, Luo W, Ji X. Carbon electrodes for K-ion batteries. *J Am Chem Soc* 2015;137:11566-9. DOI PubMed
10. Han C, Han K, Wang X, et al. Three-dimensional carbon network confined antimony nanoparticle anodes for high-capacity K-ion batteries. *Nanoscale* 2018;10:6820-6. DOI
11. Zeng S, Chen X, Xu R, et al. Boosting the potassium storage performance of carbon anode via integration of adsorption-intercalation hybrid mechanisms. *Nano Energy* 2020;73:104807. DOI
12. Tao S, Xu W, Zheng J, et al. Soybean roots-derived N, P Co-doped mesoporous hard carbon for boosting sodium and potassium-ion batteries. *Carbon* 2021;178:233-42. DOI
13. Wu X, Chen Y, Xing Z, et al. Advanced carbon-based anodes for potassium-ion batteries. *Adv Energy Mater* 2019;9:1900343. DOI
14. Xu H, Rosa AL, Frauenheim T, Zhang RQ. N-doped ZnO nanowires: surface segregation, the effect of hydrogen passivation and applications in spintronics. *Phys Stat Sol* 2010;247:2195-201. DOI
15. Zhu Y, Wang Y, Wang Y, Xu T, Chang P. Research progress on carbon materials as negative electrodes in sodium- and potassium-ion batteries. *Carbon Energy* 2022;4:1182-213. DOI
16. Ma C, Shao X, Cao D. Nitrogen-doped graphenenanosheets as anode materials for lithium ion batteries: a first-principles study. *J Mater Chem* 2012;22:8911-15. DOI
17. Liu W, Deng X, Cai S. Transport properties for carbon chain sandwiched between heteroatom-doped carbon nanotubes with different doping sites. *AIP Adv* 2016;6:075103. DOI
18. Wang Z, Selbach SM, Grande T. Van der Waals density functional study of the energetics of alkali metal intercalation in graphite. *RSC Adv* 2014;4:4069-79. DOI
19. Luo P, Zheng C, He J, et al. Structural engineering in graphite-based metal-ion batteries. *Adv Funct Mater* 2022;32:2107277. DOI
20. Li X, Li J, Ma L, et al. Graphite anode for potassium ion batteries: current status and perspective. *Energy Environ Mater* 2022;5:458-69. DOI
21. Wang D, Zhang J, Dong Y, et al. Progress on graphitic carbon materials for potassium- based energy storage. *New Carbon Mater* 2021;36:435-48. DOI
22. Costard E, Bois P, Marcadet X, Nedelcu A. QWIP and 3rd generation IR imagers. *Infrared Technol Appl 2005* ;5783:728. DOI

23. Dimiev AM, Shukhina K, Behabtu N, Pasquali M, Tour JM. Stage transitions in graphite intercalation compounds: role of the graphite structure. *J Phys Chem C* 2019;123:19246-53. DOI
24. Xing Z, Qi Y, Jian Z, Ji X. Polynanocrystalline graphite: a new carbon anode with superior cycling performance for K-ion batteries. *ACS Appl Mater Inter* 2017;9:4343-51. DOI
25. Zhang W, Liu Y, Guo Z. Approaching high-performance potassium-ion batteries via advanced design strategies and engineering. *Sci Adv* 2019;5:eaav7412. DOI PubMed PMC
26. Lei K, Li F, Mu C, et al. High K-storage performance based on the synergy of dipotassium terephthalate and ether-based electrolytes. *Energy Environ Sci* 2017;10:552-7. DOI
27. Komaba S, Hasegawa T, Dahbi M, Kubota K. Potassium intercalation into graphite to realize high-voltage/high-power potassium-ion batteries and potassium-ion capacitors. *Electrochem Commun* 2015;60:172-5. DOI
28. Sun Y, Xiao H, Li H, et al. Nitrogen/Oxygen co-doped hierarchically porous carbon for high-performance potassium storage. *Chemistry* 2019;25:7359-65. DOI
29. Luo W, Wan J, Ozdemir B, et al. Potassium ion batteries with graphitic materials. *Nano Lett* 2015;15:7671-7. DOI
30. Li J, Yi Y, Zuo X, et al. Graphdiyne/Graphene/Graphdiyne sandwiched carbonaceous anode for potassium-ion batteries. *ACS Nano* 2022;16:3163-72. DOI
31. Yuan F, Lei Y, Wang H, et al. Pseudo-capacitance reinforced modified graphite for fast-charging potassium-ion batteries. *Carbon* 2021;185:48-56. DOI
32. Capone I, Aspinall J, Lee HJ, Xiao AW, Ihli J, Pasta M. A red phosphorus-graphite composite as anode material for potassium-ion batteries. *Mater Today Energy* 2021;21:100840. DOI
33. Ma G, Huang K, Ma J, Ju Z, Xing Z, Zhuang Q. Phosphorus and oxygen dual-doped graphene as superior anode material for room-temperature potassium-ion batteries. *J Mater Chem A* 2017;5:7854-61. DOI
34. Lee B, Kim M, Kim S, et al. High capacity adsorption - dominated potassium and sodium ion storage in activated crumpled graphene. *Adv Energy Mater* 2020;10:1903280. DOI
35. Li L, Liu L, Hu Z, et al. Understanding high-rate K^+-solvent Co-intercalation in natural graphite for potassium-ion batteries. *Angew Chem Int Ed* 2020;59:12917-24. DOI
36. Vaalma C, Giffin GA, Buchholz D, Passerini S. Non-aqueous K-ion battery based on layered $K_{0.3}MnO_2$ and hard carbon/carbon black. *J Electrochem Soc* 2016;163:A1295-9. DOI
37. Liu Y, Dai H, Wu L, et al. A large scalable and low-cost sulfur/nitrogen dual-doped hard carbon as the negative electrode material for high-performance potassium-ion batteries. *Adv Energy Mater* 2019;9:1901379. DOI
38. Jian Z, Xing Z, Bommier C, Li Z, Ji X. Hard carbon microspheres: potassium-ion anode versus sodium-ion anode. *Adv Energy Mater* 2016;6:1501874. DOI
39. He X, Liao J, Tang Z, et al. Highly disordered hard carbon derived from skimmed cotton as a high-performance anode material for potassium-ion batteries. *J Power Sources* 2018;396:533-41. DOI
40. Zhang Y, Yang L, Tian Y, et al. Honeycomb hard carbon derived from carbon quantum dots as anode material for K-ion batteries. *Mater Chem Phys* 2019;229:303-9. DOI
41. Stevens DA, Dahn JR. An *in situ* small-angle X-ray scattering study of sodium insertion into a nanoporous carbon anode material within an operating electrochemical cell. *J Electrochem Soc* 2000;147:4428. DOI
42. Kim J, Lee G, Lau VW, et al. A microstructural investigation into Na-ion storage behaviors of cellulose-based hard carbons for Na-ion batteries. *J Phys Chem C* 2021;125:14559-66. DOI
43. Bommier C, Surta TW, Dolgos M, Ji X. New mechanistic insights on Na-ion storage in nongraphitizable carbon. *Nano Lett* 2015;15:5888-92. DOI PubMed
44. Li W, Zhang R, Chen Z, et al. Microstructure-dependent K^+ storage in porous hard carbon. *Small* 2021;17:e2100397. DOI
45. Wu Z, Wang L, Huang J, et al. Loofah-derived carbon as an anode material for potassium ion and lithium ion batteries. *Electrochimica Acta* 2019;306:446-53. DOI
46. Yuan F, Zhang D, Li Z, et al. Unraveling the intercorrelation between micro/mesopores and K migration behavior in hard carbon. *Small* 2022;18:e2107113. DOI
47. Wang X, Han K, Qin D, et al. Polycrystalline soft carbon semi-hollow microrods as anode for advanced K-ion full batteries. *Nanoscale* 2017;9:18216-22. DOI
48. Bin DS, Chi ZX, Li Y, et al. Controlling the compositional chemistry in single nanoparticles for functional hollow carbon nanospheres. *J Am Chem Soc* 2017;139:13492-8. DOI
49. Chen C, Wang Z, Zhang B, et al. Nitrogen-rich hard carbon as a highly durable anode for high-power potassium-ion batteries. *Energy Stor Mater* 2017;8:161-8. DOI
50. Zhang Y, Pan A, Ding L, et al. Nitrogen-doped yolk-shell-structured CoSe/C dodecahedra for high-performance sodium ion batteries. *ACS Appl Mater Inter* 2017;9:3624-33. DOI
51. Lu Y, Li D, Lyu C, et al. High nitrogen doped carbon nanofiber aerogels for sodium ion batteries: synergy of vacancy defects to boost sodium ion storage. *Appl Surf Sci* 2019;496:143717. DOI
52. Gao Y, Ru Q, Zheng M, et al. Recovery of kitchen bio-waste from spent black tea as hierarchical biomorphic carbon electrodes for ultra-long lifespan potassium-ion storage. *Appl Surf Sci* 2021;555:149675. DOI
53. Chen C, Wu M, Wang Y, Zaghib K. Insights into pseudographite-structured hard carbon with stabilized performance for high energy

K-ion storage. *J Power Sources* 2019;444:227310. DOI
54. Li J, Kaur AP, Meier MS, Cheng Y. Stacked-cup-type MWCNTs as highly stable lithium-ion battery anodes. *J Appl Electrochem* 2014;44:179-87. DOI
55. Tang Y, Zhao Y, Burkert SC, Ding M, Ellis JE, Star A. Efficient separation of nitrogen-doped carbon nanotube cups. *Carbon* 2014;80:583-90. DOI
56. Tang Y, Burkert SC, Zhao Y, Saidi WA, Star A. The effect of metal catalyst on the electrocatalytic activity of nitrogen-doped carbon nanotubes. *J Phys Chem C* 2013;117:25213-21. DOI
57. Gabaudan V, Monconduit L, Stievano L, Berthelot R. Snapshot on negative electrode materials for potassium-ion batteries. *Front Energy Res* 2019;7:46. DOI
58. Sato M. Elastic and plastic deformation of carbon nanotubes. *Procedia Eng* 2011;14:2366-72. DOI
59. Zhao X, Xiong P, Meng J, Liang Y, Wang J, Xu Y. High rate and long cycle life porous carbon nanofiber paper anodes for potassium-ion batteries. *J Mater Chem A* 2017;5:19237-44. DOI
60. Cao B, Zhang Q, Liu H, et al. Graphitic carbon nanocage as a stable and high power anode for potassium-ion batteries. *Adv Energy Mater* 2018;8:1801149. DOI
61. Wang G, Xiong X, Xie D, et al. Chemically activated hollow carbon nanospheres as a high-performance anode material for potassium ion batteries. *J Mater Chem A* 2018;6:24317-23. DOI
62. Sun J, Ma L, Sun H, et al. Design of free-standing porous carbon fibers anode with high-efficiency potassium-ion storage. *Chem Eng J* 2023;455:140902. DOI
63. Wu Y, Wu Z, Yue L, et al. Directionally Tailoring Macroporous Honeycomb-Like Structured Carbon Nanofibers toward High-Capacitive Potassium Storage. *ACS Appl Mater Inter* 2021;13:30693-702. DOI
64. Chen M, Wang W, Liang X, et al. Sulfur/Oxygen codoped porous hard carbon microspheres for high-performance potassium-ion batteries. *Adv Energy Mater* 2018;8:1800171. DOI
65. Hu X, Zhong G, Li J, et al. Hierarchical porous carbon nanofibers for compatible anode and cathode of potassium-ion hybrid capacitor. *Energy Environ Sci* 2020;13:2431-40. DOI
66. Wen J, Xu L, Wang J, et al. Lithium and potassium storage behavior comparison for porous nanoflaked Co_3O_4 anode in lithium-ion and potassium-ion batteries. *J Power Sources* 2020;474:228491. DOI
67. Tian S, Jiang Q, Cai T, et al. Graphitized electrospun carbon fibers with superior cyclability as a free-standing anode of potassium-ion batteries. *J Power Sources* 2020;474:228479. DOI
68. Ma H, Qi X, Peng D, et al. Novel fabrication of N/S Co-doped hierarchically porous carbon for potassium-ion batteries. *ChemistrySelect* 2019;4:11488-95. DOI
69. Tao L, Yang Y, Wang H, et al. Sulfur-nitrogen rich carbon as stable high capacity potassium ion battery anode: performance and storage mechanisms. *Energy Stor Mater* 2020;27:212-25. DOI
70. Wang Y, Yuan F, Li Z, Zhang D, Yu Q, Wang B. Heteroatom-doped carbon anode materials for potassium-ion batteries: from mechanism, synthesis to electrochemical performance. *APL Mater* 2022;10:030902. DOI
71. Xu Y, Zhang C, Zhou M, et al. Highly nitrogen doped carbon nanofibers with superior rate capability and cyclability for potassium ion batteries. *Nat Commun* 2018;9:1720. DOI PubMed PMC
72. Zhang M, Shoaib M, Fei H, et al. Hierarchically porous N-doped carbon fibers as a free-standing anode for high-capacity potassium-based dual-ion battery. *Adv Energy Mater* 2019;9:1901663. DOI
73. Tong H, Wang C, Lu J, et al. Energetic metal-organic frameworks derived highly nitrogen-doped porous carbon for superior potassium storage. *Small* 2020;16:e2002771. DOI
74. Chen S, Feng Y, Wang J, Zhang E, Yu X, Lu B. Free-standing N-doped hollow carbon fibers as high-performance anode for potassium ion batteries. *Sci China Mater* 2021;64:547-56. DOI
75. Zhao L, Yang H, He F, et al. Biomimetic N-doped sea-urchin-structured porous carbon for the anode material of high-energy-density potassium-ion batteries. *Electrochim Acta* 2021;388:138565. DOI
76. Gong J, Zhao G, Feng J, et al. Controllable phosphorylation strategy for free-standing phosphorus/nitrogen cofunctionalized porous carbon monoliths as high-performance potassium ion battery anodes. *ACS Nano* 2020;14:14057-69. DOI
77. Yang J, Ju Z, Jiang Y, et al. Enhanced capacity and rate capability of nitrogen/oxygen dual-doped hard carbon in capacitive potassium-ion storage. *Adv Mater* 2018;30:1700104. DOI
78. Lin X, Huang J, Zhang B. Correlation between the microstructure of carbon materials and their potassium ion storage performance. *Carbon* 2019;143:138-46. DOI
79. Share K, Cohn AP, Carter R, Rogers B, Pint CL. Role of nitrogen-doped graphene for improved high-capacity potassium ion battery anodes. *ACS Nano* 2016;10:9738-44. DOI PubMed
80. Shang Y, Duan X, Wang S, Yue Q, Gao B, Xu X. Carbon-based single atom catalyst: synthesis, characterization, DFT calculations. *Chin Chem Lett* 2022;33:663-73. DOI
81. Adekoya D, Qian S, Gu X, et al. DFT-guided design and fabrication of carbon-nitride-based materials for energy storage devices: a review. *Nanomicro Lett* 2020;13:13. DOI PubMed PMC
82. Liu Q, Hu Z, Chen M, et al. The cathode choice for commercialization of sodium-ion batteries: layered transition metal oxides *versus* prussian blue analogs. *Adv Funct Mater* 2020;30:1909530. DOI
83. Xiao Z, Meng J, Xia F, et al. K^+ modulated K^+/vacancy disordered layered oxide for high-rate and high-capacity potassium-ion

batteries. *Energy Environ Sci* 2020;13:3129-37. DOI

84. Zhao L, Zhang T, Zhao H, Hou Y. Polyanion-type electrode materials for advanced sodium-ion batteries. *Mater Today Nano* 2020;10:100072. DOI
85. Chen M, Liu Q, Zhang Y, Xing G, Chou SL, Tang Y. Emerging polyanionic and organic compounds for high energy density, non-aqueous potassium-ion batteries. *J Mater Chem A* 2020;8:16061-80. DOI
86. Liang Y, Luo C, Wang F, et al. An organic anode for high temperature potassium-ion batteries. *Adv Energy Mater* 2019;9:1802986. DOI
87. Deng Q, Pei J, Fan C, et al. Potassium salts of para-aromatic dicarboxylates as the highly efficient organic anodes for low-cost K-ion batteries. *Nano Energy* 2017;33:350-5. DOI
88. Luo Z, Liu L, Ning J, et al. A microporous covalent-organic framework with abundant accessible carbonyl groups for lithium-ion batteries. *Angew Chem Int Ed* 2018;57:9443-6. DOI
89. Wu Y, Jiang Y, Shi J, Gu L, Yu Y. Multichannel porous TiO_2 hollow nanofibers with rich oxygen vacancies and high grain boundary density enabling superior sodium storage performance. *Small* 2017;13:1700129. DOI PubMed
90. Li Y, Wang H, Wang L, et al. Mesopore-induced ultrafast Na^+-storage in T-Nb_2O_5/carbon nanofiber films toward flexible high-power Na-ion capacitors. *Small* 2019;15:e1804539. DOI
91. Cui Y, Liu W, Feng W, et al. Controlled design of well-dispersed ultrathin MoS_2 nanosheets inside hollow carbon skeleton: toward fast potassium storage by constructing spacious "houses" for K ions. *Adv Funct Mater* 2020;30:1908755. DOI
92. Wu Y, Hu S, Xu R, et al. Boosting potassium-ion battery performance by encapsulating red phosphorus in free-standing nitrogen-doped porous hollow carbon nanofibers. *Nano Lett* 2019;19:1351-8. DOI
93. Wang Q, Zhao X, Ni C, et al. Reaction and capacity-fading mechanisms of tin nanoparticles in potassium-ion batteries. *J Phys Chem C* 2017;121:12652-7. DOI
94. Chen KT, Tuan HY. Bi-Sb nanocrystals embedded in phosphorus as high-performance potassium ion battery electrodes. *ACS Nano* 2020;14:11648-61. DOI PubMed
95. Xia M, Chen B, Gu F, et al. $Ti_3C_2T_x$ MXene nanosheets as a robust and conductive tight on Si anodes significantly enhance electrochemical lithium storage performance. *ACS Nano* 2020;14:5111-20. DOI
96. Yang Q, Wang Z, Xi W, He G. Tailoring nanoporous structures of Ge anodes for stable potassium-ion batteries. *Electrochem Commun* 2019;101:68-72. DOI
97. Zhang L, Li Y, Zhang S, et al. Non-newtonian fluid state K-Na alloy for a stretchable energy storage device. *Small Methods* 2019;3:1900383. DOI
98. Eftekhari A. Low voltage anode materials for lithium-ion batteries. *Energy Stor Mater* 2017;7:157-80. DOI
99. Kim H, Kim JC, Bianchini M, Seo D, Rodriguez-garcia J, Ceder G. Recent progress and perspective in electrode materials for K-ion batteries. *Adv Energy Mater* 2018;8:1702384. DOI
100. Liu Y, Zhang N, Jiao L, Tao Z, Chen J. Ultrasmall Sn nanoparticles embedded in carbon as high-performance anode for sodium-ion batteries. *Adv Funct Mater* 2015;25:214-20. DOI
101. Yao Q, Zhu C. Advanced post-potassium-ion batteries as emerging potassium-based alternatives for energy storage. *Adv Funct Mater* 2020;30:2005209. DOI
102. Tian S, Guan D, Lu J, et al. Synthesis of the electrochemically stable sulfur-doped bamboo charcoal as the anode material of potassium-ion batteries. *J Power Sources* 2020;448:227572. DOI
103. Yang G, Ilango PR, Wang S, et al. Carbon-based alloy-type composite anode materials toward sodium-ion batteries. *Small* 2019;15:e1900628. DOI
104. Liang S, Cheng Y, Zhu J, Xia Y, Müller-buschbaum P. A chronicle review of nonsilicon (Sn, Sb, Ge)-based lithium/sodium-ion battery alloying anodes. *Small Methods* 2020;4:2000218. DOI
105. Sultana I, Rahman MM, Chen Y, Glushenkov AM. Potassium-ion battery anode materials operating through the alloying-dealloying reaction mechanism. *Adv Funct Mater* 2018;28:1703857. DOI
106. Yang GZ, Chen YF, Feng BQ, et al. Surface-dominated potassium storage enabled by single-atomic sulfur for high-performance K-ion battery anodes. *Energy Environ Sci* 2023;16:1540-7. DOI
107. Wang L, Zhao Y, Cao L, et al. CoS nanoparticle encapsulated S-doped carbon nanofiber/nanotube hybrid grown on exfoliated graphite for long-lifespan and high-rate potassium ion batteries. *Appl Surf Sci* 2022;603:154370. DOI
108. Song K, Liu C, Mi L, Chou S, Chen W, Shen C. Recent progress on the alloy-based anode for sodium-ion batteries and potassium-ion batteries. *Small* 2021;17:e1903194. DOI PubMed
109. Yi Z, Lin N, Zhang W, Wang W, Zhu Y, Qian Y. Preparation of Sb nanoparticles in molten salt and their potassium storage performance and mechanism. *Nanoscale* 2018;10:13236-41. DOI PubMed
110. Gabaudan V, Berthelot R, Stievano L, Monconduit L. Inside the alloy mechanism of Sb and Bi electrodes for K-ion batteries. *J Phys Chem C* 2018;122:18266-73. DOI
111. Shi Y, Wang L, Zhou D, Wu T, Xiao Z. A flower-like $Sb_4O_5C_{12}$ cluster-based material as anode for potassium ion batteries. *Appl Surf Sci* 2022;583:152509. DOI
112. Sultana I, Rahman MM, Mateti S, Ahmadabadi VG, Glushenkov AM, Chen Y. K-ion and Na-ion storage performances of Co_3O_4-Fe_2O_3 nanoparticle-decorated super P carbon black prepared by a ball milling process. *Nanoscale* 2017;9:3646-54. DOI
113. Liu Q, Fan L, Ma R, et al. Super long-life potassium-ion batteries based on an antimony@carbon composite anode. *Chem Commun*

2018;54:11773-6. DOI

114. Zhang W, Miao W, Liu X, Li L, Yu Z, Zhang Q. High-rate and ultralong-stable potassium-ion batteries based on antimony-nanoparticles encapsulated in nitrogen and phosphorus Co-doped mesoporous carbon nanofibers as an anode material. *J Alloys Compd* 2018;769:141-8. DOI
115. Gabaudan V, Touja J, Cot D, Flahaut E, Stievano L, Monconduit L. Double-walled carbon nanotubes, a performing additive to enhance capacity retention of antimony anode in potassium-ion batteries. *Electrochem Commun* 2019;105:106493. DOI
116. An Y, Tian Y, Ci L, Xiong S, Feng J, Qian Y. Micron-sized nanoporous antimony with tunable porosity for high-performance potassium-ion batteries. *ACS Nano* 2018;12:12932-40. DOI
117. Ko YN, Choi SH, Kim H, Kim HJ. One-pot formation of Sb-carbon microspheres with graphene sheets: potassium-ion storage properties and discharge mechanisms. *ACS Appl Mater Inter* 2019;11:27973-81. DOI
118. Ge X, Liu S, Qiao M, et al. Enabling superior electrochemical properties for highly efficient potassium storage by impregnating ultrafine Sb nanocrystals within nanochannel-containing carbon nanofibers. *Angew Chem Int Ed* 2019;58:14578-83. DOI
119. He XD, Liu ZH, Liao JY, et al. A three-dimensional macroporous antimony@carbon composite as a high-performance anode material for potassium-ion batteries. *J Mater Chem A* 2019;7:9629-37. DOI
120. Sultana I, Rahman MM, Liu J, et al. Antimony-carbon nanocomposites for potassium-ion batteries: insight into the failure mechanism in electrodes and possible avenues to improve cyclic stability. *J Power Sources* 2019;413:476-84. DOI
121. Luo W, Li F, Gaumet J, et al. Bottom-up confined synthesis of nanorod-in-nanotube structured Sb@N-C for durable lithium and sodium storage. *Adv Energy Mater* 2018;8:1703237. DOI
122. Huang Y, Wang Z, Jiang Y, et al. Conductivity and pseudocapacitance optimization of bimetallic antimony-indium sulfide anodes for sodium-ion batteries with favorable kinetics. *Adv Sci* 2018;5:1800613. DOI PubMed PMC
123. Yi Z, Qian Y, Tian J, Shen K, Lin N, Qian Y. Self-templating growth of Sb_2Se_3@C microtube: a convention-alloying-type anode material for enhanced K-ion batteries. *J Mater Chem A* 2019;7:12283-91. DOI
124. Xiong P, Wu J, Zhou M, Xu Y. Bismuth-antimony alloy nanoparticle@porous carbon nanosheet composite anode for high-performance potassium-ion batteries. *ACS Nano* 2020;14:1018-26. DOI
125. Wang T, Shen D, Liu H, Chen H, Liu Q, Lu B. A Sb_2S_3 nanoflower/MXene composite as an anode for potassium-ion batteries. *ACS Appl Mater Inter* 2020;12:57907-15. DOI
126. Yi Z, Jiang S, Du Y, et al. Coordinatively and spatially coconfining high-loading atomic Sb in sulfur-rich 2D carbon matrix for fast K^+ diffusion and storage. *ACS Mater Lett* 2021;3:790-8. DOI
127. Nguyen TH, Man MT, Do HM, Nguyen VV. Magnetic properties and electronic structure of the Sb-doped MnBi from DFT calculations. *Solid State Commun* 2021;336:114385. DOI
128. Zhao M, Zhao Q, Qiu J, Xue H, Pang H. Tin-based nanomaterials for electrochemical energy storage. *RSC Adv* 2016;6:95449-68. DOI
129. Huang B, Pan Z, Su X, An L. Tin-based materials as versatile anodes for alkali (earth)-ion batteries. *J Power Sources* 2018;395:41-59. DOI
130. Nita C, Fullenwarth J, Monconduit L, et al. Understanding the Sn loading impact on the performance of mesoporous carbon/Sn-based nanocomposites in Li-ion batteries. *ChemElectroChem* 2018;5:3249-57. DOI
131. Liu Y, Zhang N, Jiao L, Chen J. Tin nanodots encapsulated in porous nitrogen-doped carbon nanofibers as a free-standing anode for advanced sodium-ion batteries. *Adv Mater* 2015;27:6702-7. DOI PubMed
132. Sultana I, Ramireddy T, Rahman MM, Chen Y, Glushenkov AM. Tin-based composite anodes for potassium-ion batteries. *Chem Commun* 2016;52:9279-82. DOI PubMed
133. Ji B, Zhang F, Song X, Tang Y. A novel potassium-ion-based dual-ion battery. *Adv Mater* 2017;29:1700519. DOI
134. Li Z, Ding J, Mitlin D. Tin and Tin compounds for sodium ion battery anodes: phase transformations and performance. *ACC Chem Res* 2015;48:1657-65. DOI PubMed
135. Qiu D, Guan J, Li M, et al. Kinetics enhanced nitrogen-doped hierarchical porous hollow carbon spheres boosting advanced potassium-ion hybrid capacitors. *Adv Funct Mater* 2019;29:1903496. DOI
136. Han X, Liu Y, Jia Z, et al. Atomic-layer-deposition oxide nanoglue for sodium ion batteries. *Nano Lett* 2014;14:139-47. DOI
137. Ramireddy T, Kali R, Jangid MK, Srihari V, Poswal HK, Mukhopadhyay A. Insights into electrochemical behavior, phase evolution and stability of Sn upon K-alloying/de-alloying via *in situ* studies. *J Electrochem Soc* 2017;164:A2360-7. DOI
138. Gabaudan V, Berthelot R, Sougrati MT, Lippens P, Monconduit L, Stievano L. SnSb *vs.* Sn: improving the performance of Sn-based anodes for K-ion batteries by synergetic alloying with Sb. *J Mater Chem A* 2019;7:15262-70. DOI
139. Huang Z, Chen Z, Ding S, Chen C, Zhang M. Enhanced conductivity and properties of SnO_2-graphene-carbon nanofibers for potassium-ion batteries by graphene modification. *Mater Lett* 2018;219:19-22. DOI
140. Ge X, Liu S, Qiao M, et al. Enabling superior electrochemical properties for highly efficient potassium storage by impregnating ultrafine Sb nanocrystals within nanochannel-containing carbon nanofibers. *Angew Chem Int Ed* 2019;131:14720-5. DOI
141. Qin J, He C, Zhao N, et al. Graphene networks anchored with sn@graphene as lithium ion battery anode. *ACS Nano* 2014;8:1728-38. DOI
142. Huang K, Xing Z, Wang L, et al. Direct synthesis of 3D hierarchically porous carbon/Sn composites *via* in situ generated NaCl crystals as templates for potassium-ion batteries anode. *J Mater Chem A* 2018;6:434-42. DOI
143. Yang Y, Li D, Zhang J, et al. Sn nanoparticles anchored on N doped porous carbon as an anode for potassium ion batteries. *Mater*

Lett 2019;256:126613. DOI

144. Li D, Zhang Y, Sun Q, et al. Hierarchically porous carbon supported Sn_4P_3 as a superior anode material for potassium-ion batteries. *Energy Stor Mater* 2019;23:367-74. DOI
145. Du Y, Yi Z, Chen B, et al. Sn_4P_3 nanoparticles confined in multilayer graphene sheets as a high-performance anode material for potassium-ion batteries. *J Energy Chem* 2022;66:413-21. DOI
146. Li C, Bi AT, Chen HL, et al. Rational design of porous Sn nanospheres/N-doped carbon nanofibers as an ultra-stable potassium-ion battery anode material. *J Mater Chem A* 2021;9:5740-50. DOI
147. Yamamoto T, Nohira T. Tin negative electrodes using an FSA-based ionic liquid electrolyte: improved performance of potassium secondary batteries. *Chem Commun* 2020;56:2538-41. DOI PubMed
148. Liu C, Han X, Cao Y, Zhang S, Zhang Y, Sun J. Topological construction of phosphorus and carbon composite and its application in energy storage. *Energy Stor Mater* 2019;20:343-72. DOI
149. Sun J, Zheng G, Lee HW, et al. Formation of stable phosphorus-carbon bond for enhanced performance in black phosphorus nanoparticle-graphite composite battery anodes. *Nano Lett* 2014;14:4573-80. DOI
150. Sun J, Lee HW, Pasta M, et al. A phosphorene-graphene hybrid material as a high-capacity anode for sodium-ion batteries. *Nat Nanotechnol* 2015;10:980-5. DOI
151. Li W, Yang Z, Li M, et al. Amorphous red phosphorus embedded in highly ordered mesoporous carbon with superior lithium and sodium storage capacity. *Nano Lett* 2016;16:1546-53. DOI
152. Sangster JM. K-P (potassium-phosphorus) system. *J Phase Equilib Diffus* 2010;31:68-72. DOI
153. Park C, Sohn H. Black phosphorus and its composite for lithium rechargeable batteries. *Adv Mater* 2007;19:2465-8. DOI
154. Zhu Y, Wen Y, Fan X, et al. Red phosphorus-single-walled carbon nanotube composite as a superior anode for sodium ion batteries. *ACS Nano* 2015;9:3254-64. DOI
155. Sultana I, Rahman MM, Ramireddy T, Chen Y, Glushenkov AM. High capacity potassium-ion battery anodes based on black phosphorus. *J Mater Chem A* 2017;5:23506-12. DOI
156. Huang X, Liu D, Guo X, Sui X, Qu D, Chen J. Phosphorus/Carbon composite anode for potassium-ion batteries: insights into high initial coulombic efficiency and superior cyclic performance. *ACS Sustain Chem Eng* 2018;6:16308-14. DOI
157. Wu X, Zhao W, Wang H, et al. Enhanced capacity of chemically bonded phosphorus/carbon composite as an anode material for potassium-ion batteries. *J Power Sources* 2018;378:460-7. DOI
158. Xiong P, Bai P, Tu S, et al. Red phosphorus nanoparticle@3D interconnected carbon nanosheet framework composite for potassium-ion battery anodes. *Small* 2018;14:e1802140. DOI
159. Zhang W, Mao J, Li S, Chen Z, Guo Z. Phosphorus-based alloy materials for advanced potassium-ion battery anode. *J Am Chem Soc* 2017;139:3316-9. DOI
160. Yang W, Lu Y, Zhao C, Liu H. First-principles study of black phosphorus as anode material for rechargeable potassium-ion batteries. *Electron Mater Lett* 2020;16:89-98. DOI
161. Li WJ, Chou SL, Wang JZ, Liu HK, Dou SX. Simply mixed commercial red phosphorus and carbon nanotube composite with exceptionally reversible sodium-ion storage. *Nano Lett* 2013;13:5480-4. DOI PubMed
162. Sun J, Lee H, Pasta M, et al. Carbothermic reduction synthesis of red phosphorus-filled 3D carbon material as a high-capacity anode for sodium ion batteries. *Energy Stor Mater* 2016;4:130-6. DOI
163. Chang WC, Wu JH, Chen KT, Tuan HY. Red phosphorus potassium-ion battery anodes. *Adv Sci* 2019;6:1801354. DOI PubMed PMC
164. Liu D, Huang X, Qu D, et al. Confined phosphorus in carbon nanotube-backboned mesoporous carbon as superior anode material for sodium/potassium-ion batteries. *Nano Energy* 2018;52:1-10. DOI
165. Fang K, Liu D, Xiang X, et al. Air-stable red phosphorus anode for potassium/sodium-ion batteries enabled through dual-protection design. *Nano Energy* 2020;69:104451. DOI
166. Bai J, Xi B, Mao H, et al. One-step construction of N,P-codoped porous carbon sheets/CoP hybrids with enhanced lithium and potassium storage. *Adv Mater* 2018;30:e1802310. DOI
167. Wang H, Wang L, Wang L, et al. Phosphorus particles embedded in reduced graphene oxide matrix to enhance capacity and rate capability for capacitive potassium-ion storage. *Chemistry* 2018;24:13897-902. DOI
168. Xu L, Guo W, Zeng L, et al. V_3Se_4 embedded within N/P Co-doped carbon fibers for sodium/potassium ion batteries. *Chem Eng J* 2021;419:129607. DOI
169. Zhao X, Huang R, Wang T, Dai X, Wei S, Ma Y. Steady semiconducting properties of monolayer $PtSe_2$ with non-metal atom and transition metal atom doping. *Phys Chem Chem Phys* 2020;22:5765-73. DOI
170. Zhang Z, Khurram M, Sun Z, Yan Q. Uniform tellurium doping in black phosphorus single crystals by chemical vapor transport. *Inorg Chem* 2018;57:4098-103. DOI PubMed
171. Viti L, Politano A, Zhang K, Vitiello MS. Thermoelectric terahertz photodetectors based on selenium-doped black phosphorus flakes. *Nanoscale* 2019;11:1995-2002. DOI PubMed
172. Hussain F, Imran M, Rana AM, et al. Tailoring magnetic characteristics of phosphorene by the doping of Ce and Ti: a DFT study. *Phys E Low Dimens Syst Nanostruct* 2019;106:352-6. DOI
173. Duan JP, Zhang JM, Wei XM, Huang YH. Electronic, magnetic and optical properties of blue phosphorene doped with Y, Zr, Nb and Mo: a first-principles study. *Thin Solid Films* 2021;720:138523. DOI

174. Zhao W, Xu X, Wang L, et al. Boosting lifespan of conversion-reaction anodes for full/half potassium-ion batteries via multi-dimensional carbon nano-architectures confinement effect. *J Energy Chem* 2022;75:55-65. DOI

175. Sun X, Zeng S, Man R, et al. Yolk-shell structured $CoSe_2$/C nanospheres as multifunctional anode materials for both full/half sodium-ion and full/half potassium-ion batteries. *Nanoscale* 2021;13:10385-92. DOI